

# Extended finite element methods

N. Moës, J. E. Dolbow, N. Sukumar

*Ecole Centrale de Nantes, GeM Institute, 1 rue de la NOE, 44321 Nantes, France*  
*Department of Civil and Environmental Engineering, Duke University, Durham, NC 27708, USA*  
*Department of Civil and Environmental Engineering, University of California, Davis, CA 95616, USA*

## ABSTRACT

This chapter begins with a mechanical description of models involving stationary and moving interfaces. The extended finite element method (X-FEM) is then detailed for three different scenarios: crack-like interfaces, material interfaces, and free surfaces. As in the case of related methods (GFEM, PUFEM), the X-FEM relies on approximation technology that is based on a partition of unity construction. The method uses evolving enrichment functions to represent evolving geometric features and capture the local character of the solution in their vicinity. In this manner, the use of the level-set method to update such features is a natural complement to the X-FEM.

KEY WORDS: X-FEM, GFEM, PUFEM

## 1. Introduction

The finite element method (FEM) is a versatile and powerful numerical tool to solve partial differential equations. In the FEM, the problem domain is decomposed into the union of simple geometrical entities called *finite elements* over which the trial solution is represented by continuous polynomials. Since the FE interpolant is smooth in the interior of an element, the finite element method suffers from a shortcoming: *jumps* in the primary field solution or in its derivatives may only reside on element boundaries. These jumps may arise due to the presence of interfaces such as cracks, material interfaces or internal/external boundaries. Furthermore, for moving interfaces, the mesh needs to be continuously updated, with appropriate projection of field quantities for history-dependent models.

The extended finite element method (X-FEM) (Moës et al., 1999) offers the possibility to model discontinuities within finite elements. The mesh may thus be constructed independent of the location of the interfaces. A key ingredient in the X-FEM is the use of the framework of *partition of unity* (Melenk and Babuška, 1996; Babuška and Melenk, 1997), which permits the introduction of non-polynomial functions (for instance, discontinuous) into the finite element approximation. The partition of unity concept, as initially proposed in the Partition of Unity Finite Element Method (PUFEM) (Melenk and Babuška, 1996), is also adopted in the Generalized Finite Method (GFEM) (Strouboulis et al., 2001). In contrast to embedded finite element approaches (Simo et al., 1993), the X-FEM only modifies the approximation within a standard displacement-based variational formulation.

The X-FEM removes the requirement to create fitted meshes to describe internal boundaries in a model. Nonetheless, interfaces still need to be represented and captured in some manner, and the adoption of level set technology has served this need. When the X-FEM was introduced in the late 1990s for fracture models in elastic continua, level set methods were at that time booming in the fluid mechanics community in the context of finite-difference and finite-volume schemes. Within the X-FEM, an interface is modeled as the zero level set of a signed distance function, which is discretized on the mesh as a continuous field. The level set representation is in fact not mandatory for the X-FEM, but as we shall see there are numerous advantages to using it to represent interfaces.

As a powerful method to model stationary and moving interfaces, the X-FEM has been used to tackle a wide-variety of problems in different fields. In the area of modeling crack discontinuities, some of the key applications have been in fatigue, rock mechanics, hydraulic fracturing, tool machining, delamination in composites, reinforced concrete, and fragmentation. Applications with material interfaces or free boundaries include material homogenization, image-based analysis of materials, CAD technology, phase change, and topology optimization. Other type of discontinuities have also been addressed such as dislocations or flow near sharp corners.

This chapter is of course not the first endeavor to provide the state-of-the-art for the X-FEM. We direct the reader to review articles by Belytschko et al. (2009) and Fries and Belytschko (2010), and more recently, a retrospective article on the X-FEM by the authors (Sukumar et al., 2015). Monographs that provide more details on the X-FEM with an exhaustive list of references, are also available (Mohammadi, 2008; Pommier et al., 2011; Zhuang et al., 2014; Khoei, 2015).

## 2. Continuum mechanics for fixed and moving interfaces

We begin by examining continuous models for evolving interface problems in mechanics. At this stage, we may simply consider a linear elastic domain under quasi-static loading for which the strain and displacement are assumed small. The domain is denoted by  $\Omega$  and it contains, as shown in Figure 1, some features of interest to the X-FEM: a crack denoted  $\Gamma_c$  (with crack faces denoted by  $\Gamma_{c+}$  and  $\Gamma_{c-}$ ), a material interface  $\Gamma_i$ , and an internal boundary  $\Gamma_h$  describing a void. The external boundary is decomposed into a part  $\Gamma_u$  on which displacements  $\bar{\mathbf{u}}$  are imposed and a part  $\Gamma_t$  on which tractions  $\bar{\mathbf{t}}$  are imposed. We denote by  $\mathbf{u}$  the displacement field,  $\boldsymbol{\varepsilon}$  and  $\boldsymbol{\sigma}$ , the strain and stress fields, respectively.

The bulk equations that must be satisfied by these fields are (in the absence of body forces).

$$\operatorname{div} \boldsymbol{\sigma} = \mathbf{0}, \quad \boldsymbol{\varepsilon} = \frac{1}{2}(\nabla \mathbf{u} + (\nabla \mathbf{u})^\top), \quad \boldsymbol{\sigma} = \mathbf{C}(\mathbf{x}) : \boldsymbol{\varepsilon}, \quad \text{on } \Omega \quad (1)$$

where  $\mathbf{C}$  is Hooke's tensor.

Figure 1: A domain involving a crack and a material interface.

The regularity of the displacement, strain, and stress fields can be quite different in the vicinity of the geometric features  $\Gamma_c$ ,  $\Gamma_i$  and  $\Gamma_h$ .

The superscript  $-/+$  placed on some quantity  $f$  evaluated at a point  $\mathbf{x}$  on an interface has the following meaning

$$f^\pm(\mathbf{x}) = \lim_{h \rightarrow 0} f(\mathbf{x} \pm h\mathbf{n}(\mathbf{x})) \quad (2)$$

We may then define the jump and average of  $f$  across the interface

$$[f](\mathbf{x}) = f^+(\mathbf{x}) - f^-(\mathbf{x}), \quad \langle f \rangle = \frac{1}{2}(f^+(\mathbf{x}) + f^-(\mathbf{x})) \quad (3)$$

In general, the displacement field across the crack  $\Gamma_c$ , is discontinuous:

$$[\mathbf{u}]\mathbf{n} \geq \mathbf{0} \text{ on } \Gamma_c \quad (4)$$

whereas the tractions are continuous (balance of linear momentum)

$$[\boldsymbol{\sigma}]\mathbf{n} = \mathbf{0} \text{ on } \Gamma_c \quad (5)$$

Assuming frictionless crack faces, we also have

$$\langle \boldsymbol{\sigma} \rangle \mathbf{P} = \mathbf{0} \text{ on } \Gamma_c \quad (6)$$

where  $\mathbf{P}$  is the projection operator given by

$$\mathbf{P} = \mathbf{I} - \mathbf{n} \otimes \mathbf{n} \quad (7)$$

Finally, we add the condition that the crack faces may not be under tension and possibly in compression only when the crack is closed.

$$\mathbf{n} \cdot \langle \boldsymbol{\sigma} \rangle \mathbf{n} \leq 0, \quad (\mathbf{n} \cdot \langle \boldsymbol{\sigma} \rangle \mathbf{n})([\mathbf{u}] \cdot \mathbf{n}) = 0 \text{ on } \Gamma_c \quad (8)$$

Consider now the material interface  $\Gamma_i$ . If the two materials are perfectly bonded at the interface, the displacement field is continuous:

$$[\mathbf{u}] = \mathbf{0}, \quad [\boldsymbol{\sigma}]\mathbf{n} = \mathbf{0}, \text{ on } \Gamma_i \quad (9)$$

Since Hooke's tensor is discontinuous across a material interface, the above condition and the elastic constitutive law implies that the strain field is discontinuous across the interface.

Finally, if the void  $\Gamma_h$  is traction free the condition that applies is

$$\boldsymbol{\sigma}\mathbf{n} = \mathbf{0}, \text{ on } \Gamma_h \quad (10)$$

Let us summarize the type of kinematic discontinuities we need to deal with. For open cracks, both displacement components may be discontinuous as well as all components of the strain tensor. For closed cracks with frictionless contact, only the tangential displacement components may be discontinuous whereas all strain components are still possibly discontinuous. For perfectly bonded material interfaces, only the normal component of the normal strain ( $\mathbf{n} \cdot \boldsymbol{\varepsilon} \mathbf{n}$ ) is discontinuous.

The equations stated above may be recast in a variational form. At this stage, we do not consider contact on the crack faces. The set of admissible displacement fields,  $\mathcal{U}$ , and test functions  $\mathcal{U}_0$  are defined by

$$\mathcal{U} = \{\mathbf{u} \in \mathcal{V} : \mathbf{u} = \bar{\mathbf{u}}, \text{ on } \Gamma_u\} \quad (11)$$

$$\mathcal{U}_0 = \{\mathbf{u} \in \mathcal{V} : \mathbf{u} = \mathbf{0}, \text{ on } \Gamma_u\} \quad (12)$$

where  $\mathcal{V}$  is the space over  $\Omega$  which allows for the appropriate discontinuities across  $\Gamma_c$ . The variational principle reads: find  $\mathbf{u} \in \mathcal{U}$  such that

$$\int_{\Omega} \boldsymbol{\varepsilon}(\mathbf{u}) : \mathbf{C} : (\mathbf{u}^*) \, d\Omega = \int_{\Gamma_t} \bar{\mathbf{t}} \cdot \mathbf{u}^* \, d\Gamma_t, \quad \forall \mathbf{u}^* \in \mathcal{U}_0 \quad (13)$$

This variational principle yields the traction free conditions on the void boundary and crack faces, as well as the traction continuity across the material interface.

### 3. X-FEM basics

We have introduced in the previous section three major sources of discontinuities in mechanics: a discontinuity in the displacement field (cracks), in its derivative (material interface) or in the domain itself (void). Before describing the way they are handled with the X-FEM, we introduce some notations and recall the classical finite element approach.

#### 3.1. The classical finite element method

The domain of interest is first partitioned into elements  $\Omega^e$  forming a mesh covering the domain:

$$\Omega = \cup_e \Omega^e \quad (14)$$

The mesh is usually constructed to “fit” the external and internal boundaries as best as possible given the type of elements used. The element domain  $\Omega^e$  can be represented as a map from a reference configuration  $\hat{\Omega}^e$  as:

$$\Omega^e = \{\mathbf{x}(\boldsymbol{\zeta}) = \sum_{i \in I^e} \hat{N}_i(\boldsymbol{\zeta}) \mathbf{x}_i, \boldsymbol{\zeta} \in \hat{\Omega}^e\} \quad (15)$$

where  $\mathbf{x}_i$  are the nodal coordinates in physical space and  $\hat{N}_i$  are the element shape functions. The set of nodes of the element is designated by  $I^e$ . Nodes are typically located at the vertices of the element as well as on edges or faces, depending on the polynomial order of approximation. On each element, there is a one to one relation between the physical  $\mathbf{x}$  and reference coordinates  $\boldsymbol{\zeta}$ . The mapping (15) may thus be inverted to give  $\boldsymbol{\zeta}(\mathbf{x})$ .

The displacement field is approximated over the element using a linear combination of the shape functions:

$$\mathbf{u}(\boldsymbol{\zeta}) |_{\hat{\Omega}^e} = \sum_{i \in J^e} \hat{N}_i(\boldsymbol{\zeta}) \mathbf{u}_i, \quad \boldsymbol{\zeta} \in \hat{\Omega}^e \quad (16)$$

The degrees of freedom  $\mathbf{u}_i$  denote nodal displacements since, classically, the functions  $\hat{N}_i(\boldsymbol{\zeta})$  satisfy the Kronecker delta condition

$$\hat{N}_i(\boldsymbol{\zeta}(\mathbf{x}_j)) = \delta_{ij} \quad (17)$$

If the set of nodes considered for the displacement,  $J^e$ , and element geometry,  $I^e$ , are identical, the approximation is said to be isoparametric. If the former (latter) is larger than latter (former), the element is said to be sub-(super-) parametric.

The element approximation may also be written

$$\mathbf{u}(\mathbf{x})|_{\Omega^e} = \sum_{i \in J^e} \underbrace{\hat{N}_i(\boldsymbol{\zeta}(\mathbf{x}))}_{N_i(\mathbf{x})} \mathbf{u}_i, \quad \mathbf{x} \in \Omega^e \quad (18)$$

The continuity of the displacement field over the domain is ensured by enforcing the fact that elements sharing a node also share the same degree of freedom. If a crack discontinuity needs to be represented, nodes and their corresponding degrees of freedom can be duplicated along the crack surface, with one placed on each face. Such a duplication is not necessary for material interfaces, but the mesh is usually explicitly fitted to the interface geometry.

When introduced into the variational principle (13) and invoking the arbitrariness of the test functions, the approximation (16) yields a linear system of equations for the nodal displacements.

### 3.2. Recast of the finite element method

In the previous section, we did describe the finite element method in a classical manner : the approximation is given element wise and nodal degrees of freedom are vectors while the approximation functions are scalar. To introduce the X-FEM in a simple manner, we recast in this section the finite element method using nodal support concept as well as considering degrees of freedom as scalar acting on vectorial approximation functions.

The support associated with a node is the domain obtained by gathering the elements connected to the node. We denote the support of a node  $i$  by  $\omega_i$ . Over each support, approximation functions from each element may be combined to yield the so called hat functions. Typical hats are depicted in Figure 2.

Then, we shift the vectorial nature of the approximation from the degree of freedom to the approximation function.

$$\mathbf{u}(\mathbf{x})|_{\Omega} = \sum_{i \in I} \sum_{\alpha} u_i^{\alpha} \mathbf{N}_i^{\alpha}(\mathbf{x}) \quad (19)$$

where  $I$  is the set of nodes (support to be more general) in the mesh. The first summation indicates a sum over the supports, whereas the second loops over the number of degrees of freedom associated with the support. Degrees of freedom,  $u_i^{\alpha}$ , are no longer vectorial but scalar, whereas the approximation functions are no longer scalar but vectorial. To avoid the double sum in (19), we may denote  $d_i$  as any degree of freedom and  $\boldsymbol{\varphi}_i$  any approximation function

$$\{d_i\} = \{u_i^{\alpha}\}, \quad \{\boldsymbol{\varphi}_i\} = \{\mathbf{N}_i^{\alpha}\} \quad (20)$$

The finite element approximation (19) is now simply a Rayleigh-Ritz type approximation

$$\mathbf{u}(\mathbf{x})|_{\Omega} = \sum_{i \in D} d_i \boldsymbol{\varphi}_i(\mathbf{x}) \quad (21)$$

where  $D$  is the set of degrees of freedom. The stiffness matrix is readily obtained by assembly over the element

$$K_{ij} = \sum_e K_{ij}^e, \quad K_{ij}^e = \int_{\Omega^e} \boldsymbol{\varepsilon}(\boldsymbol{\varphi}_i) : \mathbf{C} : (\boldsymbol{\varphi}_j) \, d\Omega \quad (22)$$

as well as the force vector

$$F_i = \int_{\Gamma_t} \bar{\mathbf{t}} \cdot \boldsymbol{\varphi}_i \, d\Gamma \quad (23)$$

Finally, the linear system reads

$$\sum_{j \in I} K_{ij} d_j = F_i, \quad i \in I \quad (24)$$

Figure 2: Typical compactly supported finite element functions.

### 3.3. Framework of partition of unity

A key ingredient in the development of the X-FEM is the partition of unity technique introduced by Melenk and Babuška (1996), which allows one to introduce additional functions within a finite element approximation. Consider the approximation (19). How is it possible to introduce an extra displacement mode  $\mathbf{F}$  acting over  $\Omega_s \subset \Omega$ ? A naive way is to introduce it via a global approximation:

$$\mathbf{u}(\mathbf{x})|_{\Omega} = \sum_{i \in I} \sum_{\alpha} u_i^{\alpha} \mathbf{N}_i^{\alpha}(\mathbf{x}) + a \mathbf{F}(\mathbf{x}). \quad (25)$$

The above approach has a major disadvantage. The bandwidth of the stiffness matrix is now much larger, since the displacement mode  $\mathbf{F}$  that is associated with the  $a$  degree of freedom will interact with all the classical FE basis functions whose support intersects the region  $\Omega_s$ .

The main idea underlying the framework of partition of unity is to rewrite (25) as

$$\mathbf{u}(\mathbf{x})|_{\Omega} = \sum_{i \in I} \sum_{\alpha} u_i^{\alpha} \mathbf{N}_i^{\alpha}(\mathbf{x}) + \sum_{i \in S} a_i N_i(\mathbf{x}) \mathbf{F}(\mathbf{x}), \quad (26)$$

where  $S$  is the set of basis function supports that intersect the domain  $\Omega_s$ . The bandwidth is now independent of the size of  $S$ . Coefficients  $a_i$  are referred to as *enriched degrees of freedom* and the function  $\mathbf{F}$  is called an *enrichment function*. Taking all  $d_i$  as zero in (26) and choosing  $a_i$  such that

$$\sum_{i \in S} a_i N_i(\mathbf{x}) = 1 \quad \forall \mathbf{x} \in \Omega \quad (27)$$

permits  $\mathbf{F}$  to be recovered in (26). The choice  $a_i \equiv 1$  in conjunction with the partition of unity property,  $\sum_{i \in S} N_i = 1$ , ensures that (27) can be met.

### 3.4. X-FEM for a 1D discontinuity

Before describing the X-FEM enrichment strategy for a crack, we consider discontinuity modeling in one dimension. Consider the bar shown in Figure 3, which depicts two cases.

**Case a: crack located at a node** This case is treated classically with a double node. Node 2 yield two nodes  $2^-$  and  $2^+$  that share the same location but hold different degrees of freedom. Using the basis functions shown in Figure 4, the approximation reads

$$u(x) = u_1 N_1(x) + u_2^- N_2^-(x) + u_2^+ N_2^+(x) + u_3 N_3(x). \quad (28)$$

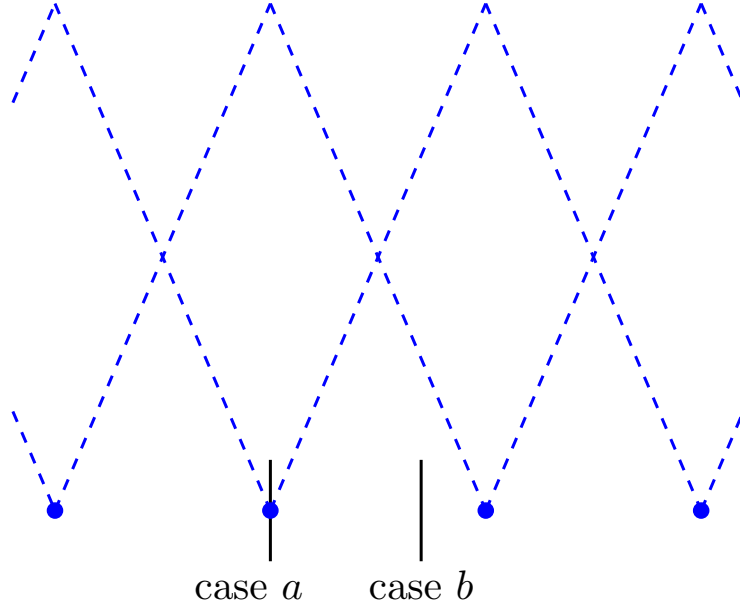


Figure 3: A bar with a crack placed at a node (case *a*) or in between two nodes (case *b*).

On using the average and jump definitions in (3), the approximation can be rewritten as

$$u(x) = \underbrace{u_1 N_1(x) + u_2 N_2(x) + u_3 N_3(x)}_{\text{classical}} + \underbrace{[u] N_2(x) H(x)}_{\text{enriched}}, \quad (29)$$

where

$$N_2(x) = N_2^-(x) + N_2^+(x), \quad u = \langle u \rangle = \frac{u_2^- + u_2^+}{2}. \quad (30)$$

The generalized Heaviside function  $H$  is shown in Figure 5. If we compare (29) to (26), we see that node 2 is enriched and the enrichment function is  $H$ .

**Case b: crack located in between two nodes** Generalizing case *a*, we write the approximation as

$$u(x) = u_1 N_1(x) + u_2 N_2(x) + u_3 N_3(x) + u_4 N_4(x) + a_2 N_2(x) H(x) + a_3 N_3(x) H(x). \quad (31)$$

Nodes 2 and 3 are both enriched with the Heaviside function. The above enrichment was introduced by Moës et al. (1999). A node is enriched if its basis function support is cut by the crack. This explains why only node 2 is enriched in case *a* and both nodes 2 and 3 are enriched in case *b*.

**Variants** Consider a single element  $[x_2, x_3]$  with a crack located at  $\xi \in (x_2, x_3)$ . The X-FEM approximation within the element is:

$$u(x) = u_1 N_1(x) + u_2 N_2(x) + a_1 N_1'(x) + a_2 N_2'(x), \quad (32)$$

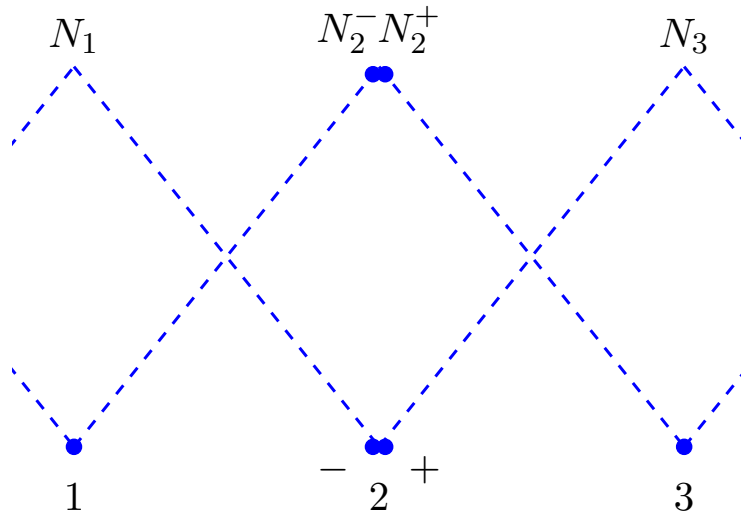


Figure 4: Double node approach for a crack located at a node.

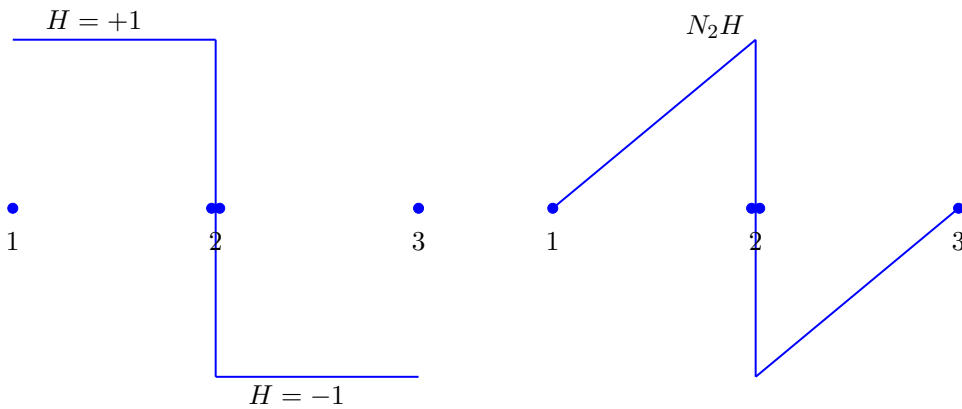


Figure 5: Generalized Heaviside (left) and its product with the  $N_2$  hat function (right).

where  $N_1'(x) = N_1(x)H(x)$  and  $N_2'(x) = N_2(x)H(x)$ . The four approximation functions are shown in Figures 7a–7d.

On combining these four functions, one can get alternative basis functions as the one proposed by Hansbo and Hansbo (2002a), which are shown in Figures 7e–7h. These were shown to be equivalent to the X-FEM basis by Areias and Belytschko (2006). The Hansbo-Hansbo representation may be interpreted as follows: the cracked element is viewed as two superposed elements. Classical approximation functions are used for each element with the

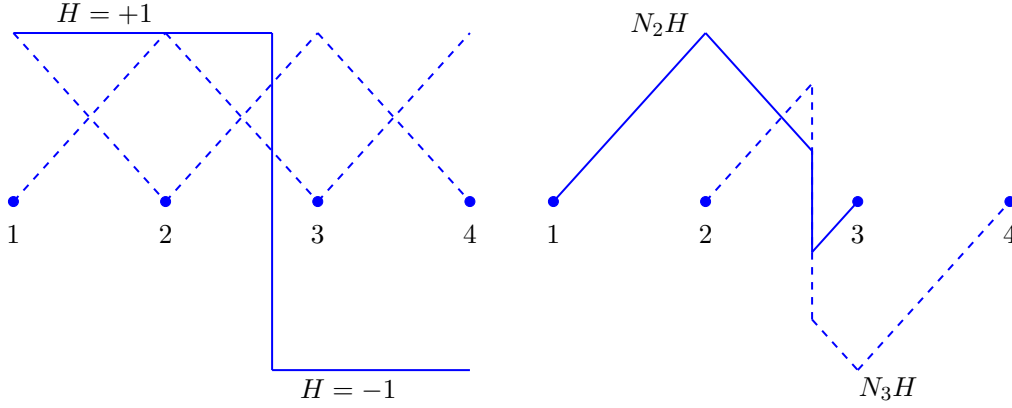


Figure 6: Heaviside (left) and approximations functions (left dashed and right) to model a crack located between nodes 2 and 3.

modification that the support of the finite element basis function is restricted to one side of the crack for one copy of the element and to the other side for the second copy of the element. This viewpoint has led to this method being referred to as the phantom-node (Song et al., 2006) or virtual-node (Molino et al., 2004) approach in the literature.

Another equivalent basis is the so-called shifted basis, which are shown in Figures 7i–7l and was proposed in Zi and Belytschko (2003). Regarding the shifted basis, the enrichment functions are limited to the elements cut by the crack. With the shifted basis, care is needed if the crack intersects a node (value of the Heaviside function at that node must be chosen in a consistent manner). Implementation issues in a given code may guide the best choice in between the three variants detailed above. The three variants yield the same solution for the displacement field.

### 3.5. X-FEM for cracks

As in one dimension, the X-FEM modeling of cracks introduces enriched degrees of freedom. Consider the crack depicted in Figure 8. Nodes that are shown with open circles have their basis function support completely cut by the crack. They will be enriched by the Heaviside function (value of +1 on one side of the crack and  $-1$  on the other side). If no further enrichment is added to the approximation, the crack will be smaller than expected because it will not be able to extend all the way to its tips. This is why a so-called tip enrichment is needed. This enrichment gives a branch-type discontinuity  $\sin(\theta/2)$ , which is discontinuous for  $\theta = \pm\pi$ . The local polar coordinates at the crack tips are indicated in Figures 9 and 10 for 2D and 3D, respectively. The X-FEM approximation as first introduced in Moës et al. (1999) is given by

$$\mathbf{u}(\mathbf{x}) = \sum_{i \in I} \sum_{\alpha} u_i^{\alpha} \mathbf{N}_i^{\alpha}(\mathbf{x}) + \sum_{i \in A \subset I} \sum_{\alpha} a_i^{\alpha} \mathbf{N}_i^{\alpha}(\mathbf{x}) H(\mathbf{x}) + \sum_{i \in B \subset I} \sum_{\alpha} \sum_{\gamma=1}^4 b_i^{\alpha, \gamma} \mathbf{N}_i^{\alpha}(\mathbf{x}) F^{\gamma}(\mathbf{x}) \quad (33)$$

We detail the notations used:

- The subset  $A \subset I$  is the set of basis function supports that are completely cut by the

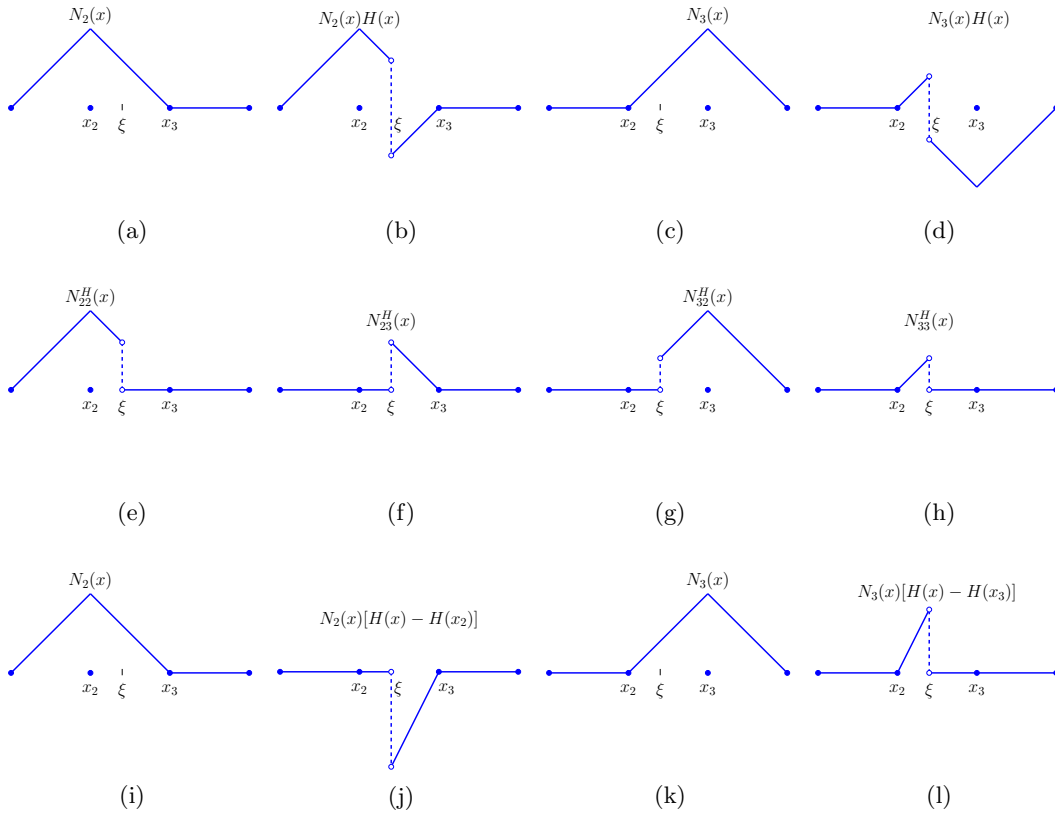


Figure 7: Basis functions for a discontinuity in one dimension. (a)–(d) X-FEM with generalized Heaviside enrichment; (e)–(h) Approach of Hansbo and Hansbo (2002a); and (i)–(l) Shifted Heaviside enrichment.

crack (open circles in Figure 8). The enriched degrees of freedom at these nodes are denoted  $a_i^\alpha$ .

- The subset  $B \subset I$  is the set of basis function supports that are enriched with the tip functions. At a minimum this set contains the support of basis functions that touch the crack tips (filled circles in Figure 8). The tip enriched degrees of freedom are denoted as  $b_i^{\alpha,\gamma}$ .
- The tip enrichment functions are

$$\{F^\gamma(\mathbf{x})\} = \sqrt{r} \left\{ \sin \frac{\theta}{2}, \cos \frac{\theta}{2}, \sin \frac{\theta}{2} \sin \theta, \cos \frac{\theta}{2} \sin \theta \right\}. \quad (34)$$

Only the first function in (34) is discontinuous across the crack. The last three functions are needed to describe the analytical asymptotic fields at the crack tip for isotropic linear elastostatic analysis.

Note that in the case of a mesh that is designed to conform to the crack, it can be shown that the first two terms of (33) yield the same approximation space as the classical double

node FEM modeling. The presence of the third term permits cracks that terminate inside an element to be modeled in the X-FEM, and it also significantly improves the accuracy of the approximation.

We may now count the number of degrees of freedom associated with each node. Let  $d$  denote the dimension of the problem ( $d = 2, 3$ ). If a node belongs to the  $I$  set,  $d$  classical degrees of freedom are attached. If this node also belongs to the set  $A$ ,  $d$  extra *Heaviside* degrees of freedom are attached. Finally, if this node belongs to the set  $B$ ,  $4d$  extra *tip* enriched degrees of freedom are attached.

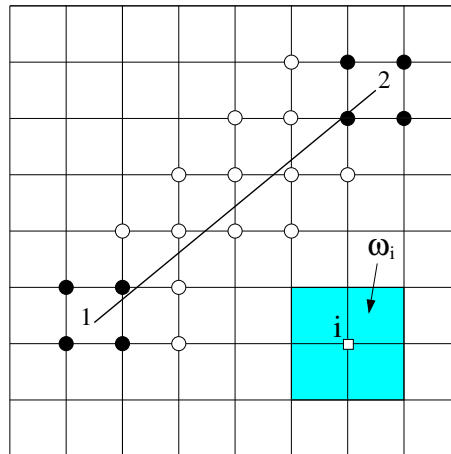


Figure 8: A crack located on a mesh and the set of nodes (open circles) to be enriched with the Heaviside and the set of nodes (filled circles) to be enriched with the tip functions.

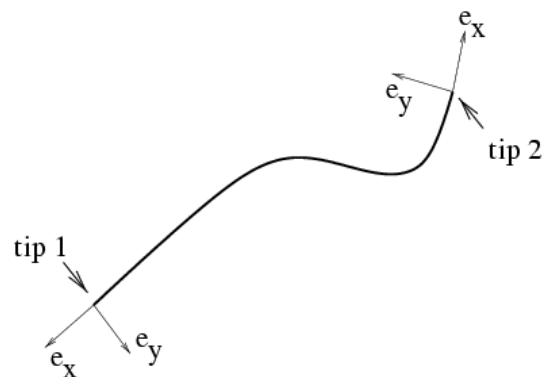


Figure 9: Local axis at the crack tips.

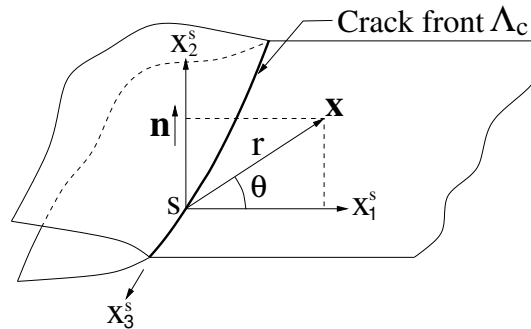


Figure 10: Local axis on the crack front in 3D.

### 3.6. Level set representation of interfaces

The X-FEM is designed to build approximations to fields in the vicinity of geometric features of interest, specifically interfaces (broadly interpreted). Ultimately the geometric structure of those interfaces needs to be described in some manner. For the X-FEM, what is needed is a tool to describe such features when they are somewhat arbitrary with respect to the underlying mesh. One approach is to adopt explicit representations for the geometry, for example in the form of parametric expressions of the curves or surfaces. While explicit approaches are tractable for relatively simple, stationary interfaces, they become cumbersome for geometrically complex or evolving interfaces. While explicit methods have been developed to deal with complicated topology changes in three dimensions, robustness has been elusive.

The level set method is an implicit way to locate an interface. The implicit concept is to consider that the interface location is the zero level set of a function defined over the whole domain (or in a narrow band around the interface). This function is usually the signed distance to the interface of interest. It can be discretized by a finite element approximation over the domain.

Consider, for example, a signed distance function to the boundary of a void in the domain. Nodes located on one side of the void will have positive values, while nodes on the other side will have negative values. Locating the void boundary is then a simple matter of finding the elements with a change of sign at their nodes, followed by finding the zero iso-contour inside these elements.

Figure 11 show the iso-zero level set of the distance function to fibers in a 4D composite. The underlying mesh is uniform. The level set function is known at each node and interpolated in between nodes with the classical finite element shape functions.

Unfortunately, crack geometries do not lend themselves to being described with a single level set (unless the crack has completely cut the domain into two parts!). Two level sets are needed. The first one gives the location of the surface on which the crack lies whereas the second one gives the extent of the crack on this surface. The iso-zero of both level set functions is depicted in Figures 12 and 13 for 2D and 3D domains, respectively. These are usually called the normal and tangential level set functions. The sign of the function  $\phi_n(\mathbf{x})$  indicates if a point  $\mathbf{x}$  is above or below the crack, and the function  $\phi_t(\mathbf{x})$  provides the distance to the crack front. On combining the two, the crack discontinuity (open set) and the crack front of the

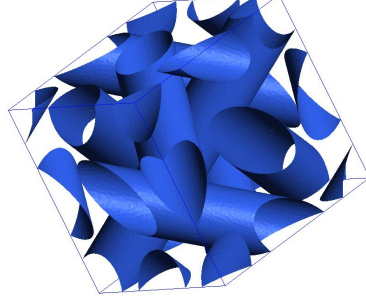


Figure 11: Iso-zero level set locating the boundaries of fibers in a 4D composite.

discontinuity are represented by the sets

$$\Gamma_c = \{\mathbf{x} : \phi_n(\mathbf{x}) = 0 \text{ and } \phi_t(\mathbf{x}) < 0\}, \quad (35a)$$

$$\Lambda_c = \{\mathbf{x} : \phi_n(\mathbf{x}) = 0 \text{ and } \phi_t(\mathbf{x}) = 0\}. \quad (35b)$$

Historically, the use of level set functions with the X-FEM for cracks was conceived in Stolarska et al. (2001), and its extension to 3D was presented in Moës and Belytschko (2002); Gravouil et al. (2002).

### 3.7. X-FEM for cracks with level sets

Now that we have introduced the level set tool to locate the crack, the enrichment function may be directly expressed in terms of the level set fields. Hence, given a point  $\mathbf{x} \in \Omega$ , there is now no need to compute the closest point on the crack-tip or crack front. Given the level set functions  $\phi_n$  and  $\phi_t$  that represent the crack surface and crack front, respectively, the enrichment functions can be expressed as:

$$H(\mathbf{x}) = \text{sign}(\phi_n), \quad r = \sqrt{\phi_n^2 + \phi_t^2}, \quad \theta = \tan^{-1} \left( \frac{\phi_n}{\phi_t} \right). \quad (36)$$

The above expressions are valid for two- and three-dimensional cracks. Using level set gradients, we may also define the local axis on the crack front:

$$\mathbf{e}_1 = \nabla \phi_n, \quad \mathbf{e}_2 = \nabla \phi_t, \quad \mathbf{e}_3 = \mathbf{e}_1 \times \mathbf{e}_2. \quad (37)$$

These local axis will be useful when defining a vectorial type enrichment for cracks (see section 5.1).

### 3.8. X-FEM for material interfaces

If a material interface is embedded within an element and the approximation fields over that element are smooth, the jump in strain across the material interface will not be properly represented. This is not of course as severe as missing the representation of a crack running

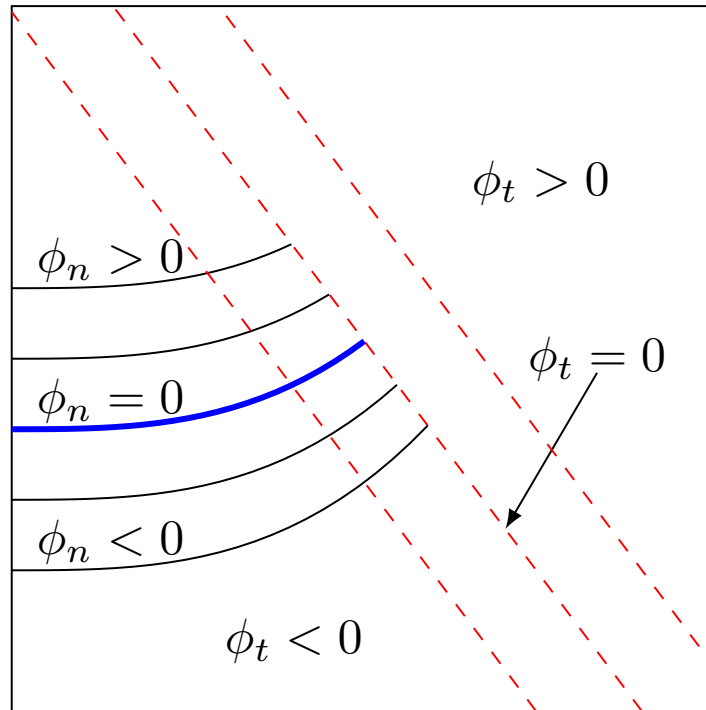


Figure 12: Level sets locating a crack in 2D.

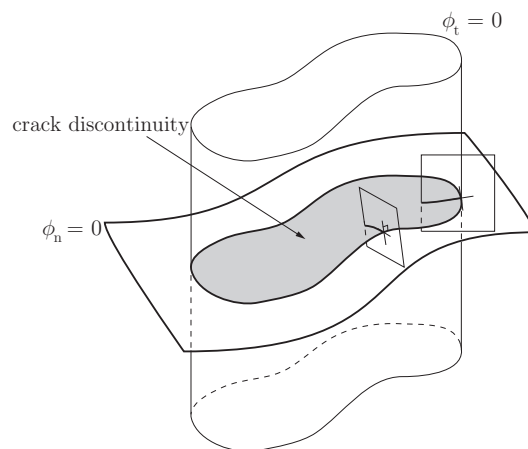


Figure 13: Level sets locating a crack in 3D.

through an element but it is yet a problem if accuracy is needed on the interface (for instance, in a analysis of debonding of this interface). The enrichment function for material interfaces needs to be continuous with discontinuous derivatives.

Several different attempts have been made to develop enrichment functions that are suitable for material interfaces. The latest being the so-called ridge enrichment Moës et al. (2003). This function is non-zero only in elements crossed by the material interface. The X-FEM approximation for a domain containing a material interface is

$$\mathbf{u}(\mathbf{x}) = \sum_{i \in I} \sum_{\alpha} u_i^{\alpha} \mathbf{N}_i^{\alpha}(\mathbf{x}) + \sum_{i \in D \subset I} \sum_{\alpha} a_i^{\alpha} \mathbf{N}_i^{\alpha}(\mathbf{x}) R(\mathbf{x}) \quad (38)$$

where  $D$  is the set of nodes for which at least one element in their support is cut by the material interface. Thus, if the material interface runs along an element boundary, no enrichment will be activated. This is appropriate because the mesh is essentially fitted to the interface in this element, and the weak discontinuities across the interface can be represented in the classical manner.

The  $R$  function is the ridge enrichment function that may be expressed easily on any element in terms of the level set function locating the material interface.

$$R(\mathbf{x}) |_{\Omega^e} = \sum_{i \in I^e} |\phi_i| N_i - \left| \sum_{i \in I^e} \phi_i N_i \right| \quad (39)$$

The ridge function is only non-zero on elements having a change of level set function sign, i.e. crossed by the material interface.

### 3.9. X-FEM for free surfaces

Taking into account voids or more generally accommodating a mesh that is larger than the domain of interest is quite straightforward with the X-FEM. The approximation does not require any specific enrichment. Supports that are completely in the void must be discarded. The remaining support set,  $E$ , is then used to build the approximation. Integrations (22) and (23) are only carried out over the physical part of the elements and boundaries, respectively.

$$\mathbf{u}(\mathbf{x}) = \sum_{i \in E} \sum_{\alpha} u_i^{\alpha} \mathbf{N}_i^{\alpha}(\mathbf{x}) H'(\mathbf{x}) \quad (40)$$

where

$$H'(\mathbf{x}) = \begin{cases} 1, & \text{if } \mathbf{x} \in \Omega \\ 0, & \text{otherwise} \end{cases} \quad (41)$$

There is no specific enrichment needed to treat a void or free surface with the X-FEM. In many respects, this separation between mesh and geometry is similar to early fictitious domain methods. For example, the fact that free surfaces can be taken into account on non-matching boundaries was noted very early by Hyman (1952) in the context of finite difference methods.

## 4. Implementation of the X-FEM

### 4.1. Numerical computation of weak form integrals

On using trial and test functions of the form (33), (38) or (40), in the weak form (13), we obtain the discrete set of equations (24). The entries of the stiffness matrix are given by integrals with

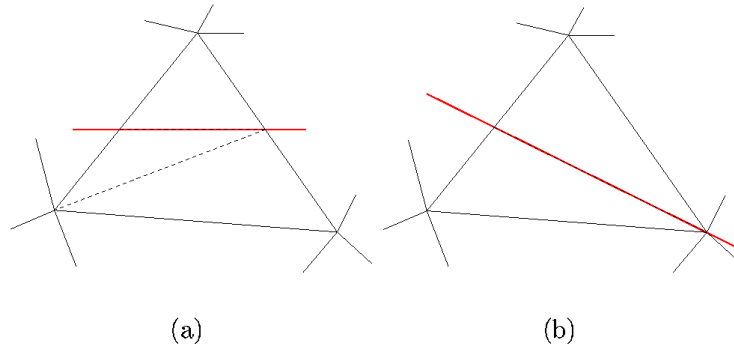


Figure 14: Two scenarios of the iso-zero level set cut of a triangle.

integrands that are discontinuous across the crack or material interface. Also, if the element contains a void, the integral is restricted to the non-void part of the element. To accurately evaluate these contributions to the stiffness matrix, appropriate procedures are needed to perform the numerical integration. As advocated initially in Moës et al. (1999); Sukumar et al. (2000), the vast majority of approaches that may be found in the X-FEM literature on this matter advocates the use of the decomposition of the element into subcells that conform to the interface. On each subcell, the integrand is now continuous and if we put aside the tip enrichment, the integrand is even polynomial for structured or Delaunay finite element meshes. It is worth pointing out that this procedure is not equivalent to remeshing, since no additional degrees of freedom accrue and in addition, there are no restrictions placed on the shape of these subcells. Consider an interface that intersects an element, with its location given by a level set function that is interpolated over the element. On triangles and tetrahedra, the cut is a plane: Figures 14 and 15 depict the possible cuts in 2D and 3D, respectively.

In 2D, an enriched element is decomposed into a collection of triangles, with the crack conforming to the boundary edges of the triangles. The partitioning is relatively easy to implement in 2D, but for multiple cracks with kinks in 3D, more sophisticated computational geometric algorithms are needed for an efficient and robust implementation. To avoid the need for partitioning the elements, algorithms for polynomial-precision quadrature rules that integrate discontinuous functions on either side of the crack have been proposed (Holdych et al., 2008; Mousavi and Sukumar, 2010b; Ventura and Benvenuti, 2015), but these and further advances are the subject of ongoing research.

Elements that contain the crack-tip in two dimensions or those that intersect the crack front in three dimensions require special treatment. A higher-order tensor-product Gauss quadrature rule as adopted in Moës et al. (1999) and Sukumar et al. (2000) suffice for coarse-mesh accuracy. However, to demonstrate robustness of the method and to establish convergence for geometric enrichment (Laborde et al., 2005; Béchet et al., 2005), the weakly singular integrands must be accurately integrated to ensure optimal asymptotic convergence. Use of Gauss quadrature limits the accuracy for such integrals, and hence in two dimensions the Duffy transformation (Duffy, 1982; Laborde et al., 2005) and a

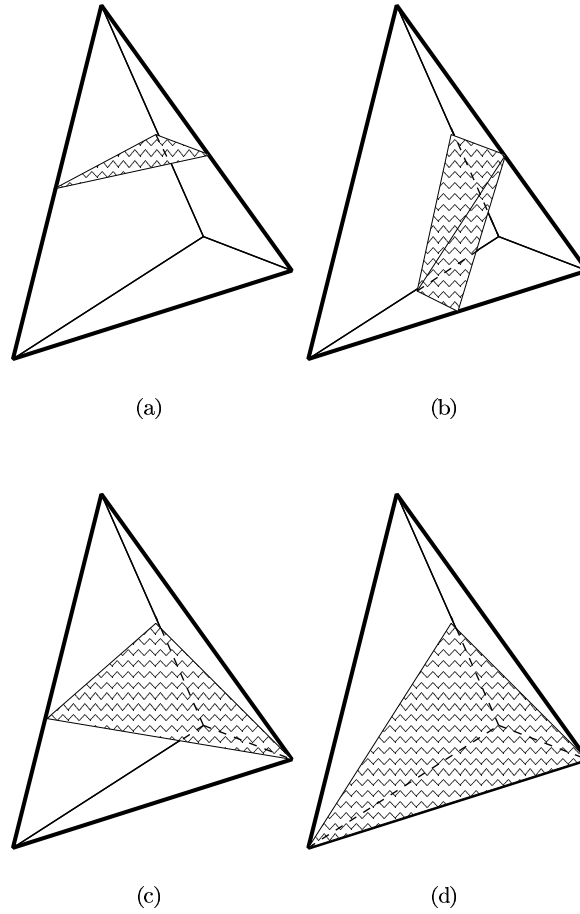


Figure 15: Four scenarios for the cut of a tetrahedron by an iso-zero level set.

parabolic transformation (Béchet et al., 2005) were introduced. Mousavi and Sukumar (2010a) generalized the Duffy transformation to integrate weakly singular integrands. In this approach, when the crack-tip is located within an element, the element is partitioned into triangles with the crack-tip located at a vertex of each triangle. An affine transformation is first used to map each triangle to the standard triangle  $T_0$  shown in Figure 16. Then, the unit square is mapped to the standard triangle via the transformation:

$$(u, v) \rightarrow (x, y) : x = u^\beta, y = xv = u^\beta v, \quad (42)$$

where  $\beta \in \mathbb{Z}^+$ . Consider integrating  $f(\mathbf{x}) := g(\mathbf{x})r^{-\alpha}$  over  $T_0$ , where  $r = \sqrt{x^2 + y^2}$  and  $g(x, y)$  is a bivariate polynomial. Then, on applying (42), the kernel becomes

$$K(u, v) := \frac{g(u^\beta, u^\beta v)\beta u^{2\beta-1-\alpha\beta}}{\sqrt{1+v^2}}. \quad (43)$$

The parameter  $\beta$  is selected so that the exponent of  $u$  in (43) is the smallest positive integer. For  $\alpha = 1$ , the  $1/r$  singularity is removed with  $\beta = 1$  (Duffy transformation), whereas for  $1/\sqrt{r}$  ( $\alpha = 1/2$ ),  $\beta = 2$  is optimal. For elastic fracture, since terms involving  $1/r$  and  $1/\sqrt{r}$  appear in the stiffness matrix for the X-FEM, this approach has shown to be accurate in two dimensions (Mousavi and Sukumar, 2010b; Minnebo, 2012; Cano and Moreno, 2015). This numerical integration scheme to eliminate power singularities in the weak form integrals can also find application in problems such as hydraulic fracture (Gordeliy and Peirce, 2015) and crack impinging a bimaterial interface (Huang et al., 2003). For a crack front that represents a line singularity, Minnebo (2012) has presented extensions of the Duffy and parabolic transformation schemes to integrate singular enrichment functions in 3D.

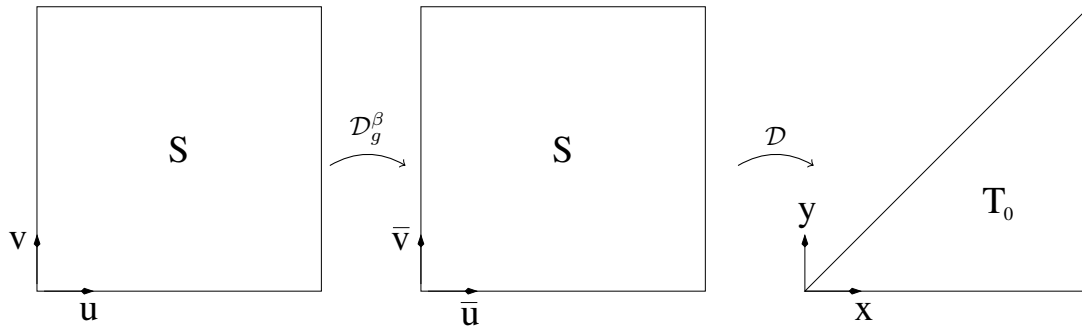


Figure 16: Transformations from the unit square to the standard triangle. The Duffy transformation  $\mathcal{D} : S \rightarrow T_0$  maps the unit square to the standard triangle, which is followed by a power transformation  $\mathcal{D}_g^\beta : S \rightarrow S$  that maps the square onto itself. The composite map from  $\mathbf{u} \rightarrow \mathbf{x}$  is:  $x = u^\beta$ ,  $y = u^\beta v$ , where  $\beta \in \mathbb{Z}^+$ .

#### 4.2. Update of level sets for moving interfaces

We discuss algorithms needed to update a physical boundary located by one or two level set functions. We begin with boundaries such as closed material interfaces that can be represented using a single level set function, and then move to cracks that require two level set functions for their representation and to update their location.

**4.2.1. Single level set update** Consider an initial contour  $\gamma$  ( $t = 0$ ) at  $t = 0$  located by a level set function  $\phi$  representing the signed distance function to this contour:

$$\phi(\mathbf{x}, t = 0) = \min_{\mathbf{x}_\gamma \in \gamma(t=0)} \pm \|\mathbf{x} - \mathbf{x}_\gamma\|. \quad (44)$$

Let us assume that the normal velocity  $v_n$  of the front is known. There are two possible choices of equations to update the level set field. These equations only need to be applied in a narrow band  $B$  in the vicinity of the contour  $\phi = 0$ , since this interface is not expected to move very far over the small time increment  $\Delta t$  for which the equations are solved.

The first equation, is an initial boundary value problem:

$$\frac{\partial \phi}{\partial t} + v_n \|\nabla \phi\| = 0, \quad \text{given } \phi(\mathbf{x}, t = 0). \quad (45)$$

The location of the interface at  $t = \Delta t$  is given by the level set  $\phi(\mathbf{x}, \Delta t) = 0$ . Temporal and spatial discretization of (45) are thoroughly discussed in the literature for uniform and nonuniform grids, see for instance, Sethian (1999). The update scheme is explicit, and does not require any matrix solve. The computational time is thus proportional to the number of nodes,  $N$ , in the narrow band. For stability, the time step  $\Delta t$  needs to satisfy a CFL condition, namely,

$$\Delta t \leq \min_B(\Delta x/v_n), \quad (46)$$

where  $\Delta x$  is a measure of the element size.

The second possible equation, which is only applicable if the normal velocity  $v_n$  has the same sign along  $\gamma$ , is a boundary-value problem called the Eikonal equation:

$$\|\nabla\psi\| = \frac{1}{v_n}, \quad \psi = 0 \text{ on } \gamma \text{ (} t = 0 \text{)}. \quad (47)$$

The value of  $\psi$  at a point  $\mathbf{x}$  indicates the time it takes for the front moving at velocity  $v_n$  to reach point  $\mathbf{x}$ . The location of  $\gamma$  ( $t > 0$ ) is given by the level set  $\psi = t$ . A very efficient algorithm to solve the Eikonal equation is the fast marching scheme. It requires more operations than the algorithm for the level set equation (45) —  $N \log(N)$  versus  $N$  — but has no CFL condition on the time step. Hence, much larger time steps can be used in the fast marching method.

**(Re)initialization of the signed distance function** The level set equation (45) requires the knowledge of the level set field at  $t = 0$ . This may be obtained by explicitly computing the signed distance to the initial contour or by solving the following time evolution problem until a stationary solution is reached:

$$\frac{\partial\phi}{\partial\tau} + \text{sign}(\phi)(\|\nabla\phi\| - 1) = 0. \quad (48)$$

The role of  $\text{sign}(\phi)$  is to ensure that the zero level set of  $\phi$  is not affected. Note that the above is quite different from (45) since it is solved with a virtual time  $\tau$  until a stationary solution is reached and not over a small time increment. Herein, a CFL condition also applies. The initial condition for (48) must at least have the correct iso-zero contour.

Another way to (re)initialize is to use fast marching for the Eikonal equation. To this end, we first solve

$$\|\nabla\phi\| = 1. \quad (49)$$

Since the velocity is unity everywhere, the time it takes to reach a point away from the contour is the distance to this contour. Both (48) and (49) may be used to reinitialize the level set functions between update steps. Reinitialization ensures that as the front propagates, the level set field remains a signed distance function, i.e., it satisfies (49).

**Velocity extension** Equations (45) and (47) require the knowledge of the normal velocity over the domain and not just in the vicinity of the interface. We need an extension of  $v_n$  from the iso-zero contour to the narrow band. The extension must flow along the level set gradient:

$$\nabla v_n \cdot \nabla\phi = 0. \quad (50)$$

This normality condition ensures that (45) does not modify relation (49).

As for the (re)initialization, the construction of a velocity satisfying (50) may be done in one of two ways: either by solving an initial boundary value problem or a boundary-value problem. For the first choice, we have

$$\frac{\partial v_n}{\partial \tau} + \text{sign}(\phi) \frac{\nabla \phi}{\|\nabla \phi\|} \cdot \nabla v_n = 0. \quad (51)$$

A better way to solve (50) is to use a fast marching method. Indeed, as this algorithm proceeds to solve (49), it has all the information needed to propagate the velocity matching condition (50). For planar cracks, it suffices to update a single level set function. The fast marching method was combined with the X-FEM for single planar cracks in Sukumar et al. (2003) and then extended for multiple planar cracks in Chopp and Sukumar (2003).

*4.2.2. Double level set update: crack growth* We consider three-dimensional crack propagation. Two-dimensional crack propagation may be seen as a particular case of 3D, or alternatively, 2D crack growth may be simply dealt with by adding segments to an existing crack without requiring the use of level set functions. The first level set based algorithm to propagate 3D cracks was conceived in (Gravouil et al., 2002). It was purely based on the level set update equation. It is reproduced below. The front velocity is decomposed into an in plane velocity  $v_t$  (velocity of growth of the crack in its plane) and an out of plane velocity  $v_n$ .

1. extension of  $\phi_n$  in the region  $\phi_t \geq 0$  along the gradient  $\nabla \phi_t$ :

$$\frac{\partial \phi_t}{\partial \tau} + \text{sign}(\phi_n) \frac{\nabla \phi_n}{\|\nabla \phi_n\|} \cdot \nabla \phi_t = 0. \quad (52)$$

2. extension of  $v_t$  to the domain:

$$\frac{\partial v_t}{\partial \tau} + \text{sign}(\phi_t) \frac{\nabla \phi_t}{\|\nabla \phi_t\|} \cdot \nabla v_t = 0, \quad \frac{\partial v_t}{\partial \tau} + \text{sign}(\phi_n) \frac{\nabla \phi_n}{\|\nabla \phi_n\|} \cdot \nabla v_t = 0. \quad (53)$$

3. extension of  $v_n$  to the domain:

$$\frac{\partial v_n}{\partial \tau} + \text{sign}(\phi_n) \frac{\nabla \phi_n}{\|\nabla \phi_n\|} \cdot \nabla v_n = 0, \quad \frac{\partial v_n}{\partial \tau} + \text{sign}(\phi_t) \frac{\nabla \phi_t}{\|\nabla \phi_t\|} \cdot \nabla v_n = 0. \quad (54)$$

4. adjustment to prevent modification to the previous crack surface

$$\bar{v}_n = \begin{cases} 0 & \text{if } \phi_t \leq 0 \\ \frac{v_n \phi_t}{v_t \Delta t} & \text{else} \end{cases}. \quad (55)$$

5. update and reinitialize  $\phi_n$ :

$$\frac{\partial \phi_n}{\partial t} + \bar{v}_n \|\nabla \phi_n\| = 0, \quad \frac{\partial \phi_n}{\partial \tau} + \text{sign}(\phi_n) (\|\nabla \phi_n\| - 1) = 0. \quad (56)$$

6. update  $\phi_t$ :

$$\frac{\partial \phi_t}{\partial t} + v_t \|\nabla \phi_t\| = 0. \quad (57)$$

7. orthogonalize and reinitialize  $\phi_t$ :

$$\frac{\partial \phi_t}{\partial \tau} + \text{sign}(\phi_n) \frac{\nabla \phi_n}{\|\nabla \phi_n\|} \cdot \nabla \phi_t = 0, \quad \frac{\partial \phi_t}{\partial \tau} + \text{sign}(\phi_t) (\|\nabla \phi_t\| - 1) = 0. \quad (58)$$

Equations involving the virtual time  $\tau$  must be solved until a stationary solution is reached, whereas the other equations are solved over a time step  $\Delta t$ .

The algorithm above may give the impression that it is possible to satisfy both the orthogonality of the level set gradients and their unit norm. As pointed out by Dufloy (2007), this is not possible, i.e., conditions below are incompatible:

$$\|\nabla\phi_n\| = 1, \quad \|\nabla\phi_t\| = 1, \quad \nabla\phi_n \cdot \nabla\phi_t = 0. \quad (59)$$

The fast marching method has also been used to simulate three-dimensional nonplanar crack growth (Sukumar et al., 2008; Shi et al., 2010). In this approach, first the distance function  $\rho$  that solves  $\|\nabla\rho\| = 1$  is obtained; then, the velocity  $\mathbf{F}$  is mapped onto grid points near the front and then extended to the whole domain by solving:  $\nabla\mathbf{F} \cdot \nabla\rho = 0$ . Given the level set functions  $\phi_n^m$  and  $\phi_t^m$  at step  $m$ , they are advanced in time to step  $m + 1$  using vector decompositions that consider the velocity of propagation, the distance function  $\rho$ , and the fact that  $\phi_n^{m+1}$  and  $\phi_t^{m+1}$  must remain orthogonal. Further details on the update are provided in Sukumar et al. (2008); in Shi et al. (2010), the update is restricted to a narrow band in the vicinity of the crack. Geometric approaches to update the level set functions within the X-FEM have also been pursued: Ventura et al. (2003) did so for two-dimensional crack growth and Colombo and Massin (2010) treated three-dimensional nonplanar crack growth using a geometrical approach for velocity extension and upwind finite-difference discretization of the Hamilton-Jacobi equations.

## 5. X-FEM advanced

The goal of the previous section was to give a quick overview of the capabilities of the X-FEM to model displacement discontinuities in the field itself (crack) in its derivative (material interface) or at the domain boundary. In this section, we discuss several topics in more detail.

### 5.1. Variation in the enrichment

The X-FEM approximation for cracks (33) has seen several interesting evolutions over the years after its initial inception in 1999. The first one deals with the choice of the enrichment sets  $A$  and  $B$ , corresponding to crack interiors and tips, respectively.

Regarding the set  $A$ , the rule is: every support completely cut by the crack must be enriched by the Heaviside. This approach to Heaviside enrichment is in fact the only rule that makes sense. This can be demonstrated by examining the alternatives:

- if a support not completely cut by the crack is enriched with the Heaviside, the displacement discontinuity will extend beyond the crack geometry.
- if a support is not cut at all by the crack and is enriched, the enriched function will be linearly dependent with the classical one (the Heaviside having a uniform value of +1 or -1 over the support), and the linear algebraic system will be singular
- if a support completely cut by a crack is not enriched, the displacement discontinuity is not adequately represented.

We note that the above rule must hold true for any classical function in the approximation, whatever its degree (linear, parabolic, cubic, ...).

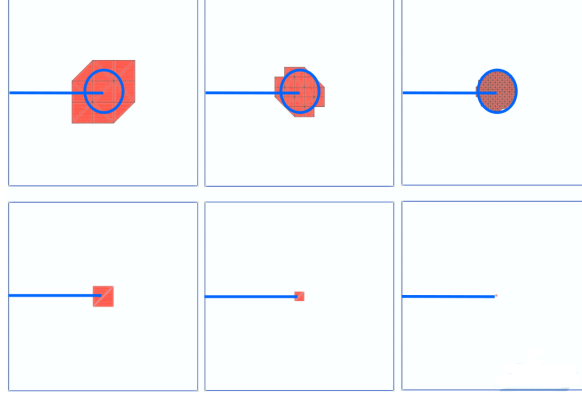


Figure 17: Extent of the geometrical (top line) and topological (bottom line) enrichment zone as the mesh size decreases.

Regarding the  $B$  set (tip/front enrichment) we have more flexibility. Two types of enrichment strategies exist. They were introduced simultaneously in (Laborde et al. (2005) and Béchet et al. (2005)). The so-called topological enrichment consists of enriching a set of layers around the tip/front. With this enrichment strategy, the measure of the enriched zone shrinks to zero in the asymptotic process of the mesh size going to zero (see bottom of Figure 17). We can thus expect that the benefit of the enrichment will vanish in the limit. This is indeed observed in the error convergence analysis.

On the contrary, the geometrical enrichment strategy enriches all nodes located with some distance to the crack front/tip. The size of the enrichment zone is thus mesh independent (top of Figure 17). The convergence behavior is now much better and the benefit of the enrichment is not lost asymptotically. The trade-off however is a larger number of degrees of freedom and an increase in the conditioning of the linear system.

Several strategies may be designed to keep the benefit of the geometrical enrichment while alleviating the associated increase in the conditioning of the linear algebraic system. These strategies all strive to reduce the number of enriched degrees of freedom while preserving the size of the domain over which the enrichment acts.

The first one, introduced in the 2D setting, is the cut-off function approach (cite). The idea is to reduce the enriched degrees of freedom to 2 representing the mode 1 and mode 2 displacement fields (check).

The second one called vectorial enrichment (useful both in 2D and 3D settings) follows the same principle but on a nodal basis. The 8 (12) degrees of freedom in 2D (3D) per node are reduced to only 2 (3) degrees of freedom. The X-FEM approximation for the vectorial enrichment reads in 3D

$$\mathbf{u}(\mathbf{x}) = \sum_{i \in I} \sum_{\alpha} u_i^{\alpha} \mathbf{N}_i^{\alpha}(\mathbf{x}) + \sum_{i \in ACI} \sum_{\alpha} a_i^{\alpha} \mathbf{N}_i^{\alpha}(\mathbf{x}) H(\mathbf{x}) + \sum_{i \in BCI} \sum_{\gamma=1}^3 b_i^{\gamma} N_i(\mathbf{x}) \mathbf{F}^{\gamma}(\mathbf{x}) \quad (60)$$

Compared to (33), only the last term has been modified. The enrichment functions are now vectorial and correspond to pure mode 1, 2 and 3:

$$\mathbf{F}^1 = \frac{1}{2\mu} \sqrt{\frac{r}{2\pi}} \left( \cos \frac{\theta}{2} (\kappa - \cos \theta) \mathbf{e}_1 + \sin \frac{\theta}{2} (\kappa - \cos \theta) \mathbf{e}_2 \right) \quad (61)$$

$$\mathbf{F}^2 = \frac{1}{2\mu} \sqrt{\frac{r}{2\pi}} \left( \sin \frac{\theta}{2} (\kappa + 2 + \cos \theta) \mathbf{e}_1 + \cos \frac{\theta}{2} (\kappa - 2 + \cos \theta) \mathbf{e}_2 \right) \quad (62)$$

$$\mathbf{F}^3 = \frac{1}{2\mu} \sqrt{\frac{r}{2\pi}} \sin(\theta/2) \quad (63)$$

where  $\mu = \frac{E}{2(1+\nu)}$ ,  $E$  is Young's modulus and  $\nu$  Poisson's ratio. For plane strain conditions in 3D (check),  $\kappa = 3 - 4\nu$  and for plane stress  $\kappa = \frac{3-\nu}{1+\nu}$ . Note that if the crack is located with level sets, the enrichment function may be computed directly using (36) and (37). The expression

$$K^\gamma(\mathbf{x}) = \sum_{i \in BCI} b_i^\gamma N_i(\mathbf{x}) \quad (64)$$

evaluated along the crack front (3D) or at the crack tip (2D) provides direct information about the stress intensity factors. It was shown by Chevaugeon in 2D that this estimation is not as accurate as the energetic domain integral approach (one order less in convergence rate).

### 5.2. Extraction of the SIFs

Stress intensity factors are usually calculated by post-processing the calculated displacement, strain, and stress fields. For stress intensity factor computations with extended finite elements, the use of crack-tip flux integrals leads to better accuracy than displacement or stress extrapolation techniques. In particular, domain forms of the  $J$ -integral and associated interaction integrals are most commonly used. Interaction integrals are used to extract individually each of the stress intensity factor along the front.

Consider an arbitrary point  $s$  on a crack front (Figure 10). For simplicity, we assume the crack is under pure mode  $I$ . The mode- $I$  stress intensity factor is given by

$$K_I(s) = \sqrt{\frac{J(s)E}{1-\nu^2}} \quad (65)$$

With the normal to the crack front (and in the crack plane) oriented along the  $\hat{x}_1$ -axis of a local coordinate system, the pointwise  $J$ -integral is given by

$$J(s) = \lim_{\Gamma \rightarrow 0} \int_{\Gamma(s)} H_{1\beta} \mathbf{n}_\beta d\Gamma, \quad (\beta = 1, 2) \quad (66)$$

where

$$H_{1j} = W \delta_{ij} - \sigma_{ij} u_{i,1} \quad (i, j = 1, 2, 3) \quad (67)$$

For linear elastostatics, in the absence of body forces and material inhomogeneities, and assuming traction-free crack surfaces, the volume form of the domain integral is given by Destuynder et al. (1983)

$$J(s) = -\frac{\int_V (H_{kj} q_{k,j} + H_{kj,j} q_k) dV}{\int_{L_c} l_k n_k ds} \quad (68)$$

where  $V$  is a volume enclosing the crack front,  $n_k(s)$  are components of the in-plane unit outward normal at  $s$ ,  $l_k(s)$  are components of an arbitrary unit vector at  $s$  lying in the plane of the crack, and  $L_c$  is the perturbed segment (virtual extension) along the crack front. The vector field  $q_k$  is defined in  $V$  as

$$q_k = \begin{cases} l_k & \text{on } S_t \\ 0 & \text{on } S_0 \\ \text{arbitrary} & \text{otherwise} \end{cases} \quad (69)$$

In order to evaluate (66), a virtual extension domain is required around the point  $s$  on the crack front. Typically, in fracture analysis with classical finite elements, the mesh is constructed so that the virtual extension domain is the union of finite elements in the vicinity of the point  $s$ . Since the crack is not explicitly fitted by the mesh with the X-FEM, a convenient collection of element domains near the crack tip is often not readily available. For two-dimensional implementations of the X-FEM, elements that are within a characteristic distance of the crack-tip are included in the virtual extension domain. This approach does not readily extend to three dimensions, however.

For extracting SIFs in three-dimensional problems with the X-FEM, the standard approach to constructing the virtual extension domain is to construct an independent grid of hexahedral cells around the point  $s$ . Let the perturbed segment ( $L_c$ ) along the crack front be parameterized by the curvilinear coordinate  $s : R^3 \rightarrow [0; L_c]$ . Consider the evaluation of the domain integral at a point  $s$  on the crack front. The dimensions of the virtual extension domain are:  $L_1$ ,  $L_2$ , and  $L_3$  along the coordinate directions in the local system defined at the crack front. The point  $s$  is located at the origin of the local orthogonal coordinate system (Figure ?). The  $x_2$ -axis is contained in the plane of the crack and is tangential to the crack front at  $s$ . The  $J$ -domain is subdivided into a set of hexahedral cells, and then a high-order quadrature rule is used in each. In three-dimensional fracture, the denominator in (66) is approximated by the formula  $(L_2^+ + L_2^-)/2$ , where  $L_2^+$  and  $L_2^-$  are the domain lengths on either side of  $s$  in the local  $x_2$ -direction.

Typically, the components  $q_k$  are also given in the local coordinate system, with only the  $x_1$  component being non-zero. It is often taken to be a function that decays linearly down to zero in each of the coordinate directions, e.g.

$$q_1(x_1, x_2, x_3) = \left(1 - \frac{2|x_1|}{L_1}\right) \left(1 - \frac{2|x_2|}{L_2}\right) \left(1 - \frac{2|x_3|}{L_3}\right) \quad (70)$$

At each cell quadrature point, it is necessary to locate the position of the point in the original mesh and then extract the needed quantities such as the strain energy density. We note that these fields are discontinuous across element boundaries, and as such there is error associated with the cell quadrature. SIFs obtained with this approach tend to exhibit oscillations. These oscillations are also present using the finite element method and meshes that are not graded along the crack front

To alleviate oscillations, recent works promote the use of a global approach. Instead of trying to extract point-wise values of the SIFs along the front. The SIFs variation along the front is expressed in terms of a global approximation. Coefficients of the approximation are obtained by solving a linear system. This technique is based on the domain form of the energy integrals Destuynder et al. (1983) and was initially developed in the FEM context.

### 5.3. Convergence rate

We now discuss the accuracy of the X-FEM to approximate solutions to problems in linear elastic fracture mechanics. Consider a square domain with a straight crack in plane strain subjected to pure mode I traction conditions on its outer boundary. The exact solution is known and shown with a scale factor in Figure 18. Young's modulus is taken as 1 and Poisson's ratio as 0. The square side length is 1. A convergence analysis is performed with a uniform grid which is recursively refined. The energy norm error,  $\epsilon$ , measuring the distance between the exact,  $\boldsymbol{\sigma}^{\text{ex}}, \mathbf{u}^{\text{ex}}$ , and approximated field  $\boldsymbol{\sigma}, \mathbf{u}$

$$\epsilon = \left( \frac{\int_{\Omega} (\boldsymbol{\sigma} - \boldsymbol{\sigma}^{\text{ex}}) : \mathbf{C}^{-1} : (\boldsymbol{\sigma} - \boldsymbol{\sigma}^{\text{ex}}) \, d\Omega}{\int_{\Omega} \boldsymbol{\sigma}^{\text{ex}} : \mathbf{C}^{-1} : \boldsymbol{\sigma}^{\text{ex}} \, d\Omega} \right)^{1/2} \quad (71)$$

$$= \left( \frac{\int_{\Omega} \boldsymbol{\varepsilon}(\mathbf{u} - \mathbf{u}^{\text{ex}}) : \mathbf{C} : \boldsymbol{\varepsilon}(\mathbf{u} - \mathbf{u}^{\text{ex}}) \, d\Omega}{\int_{\Omega} \boldsymbol{\varepsilon}(\mathbf{u}^{\text{ex}}) : \mathbf{C} : \boldsymbol{\varepsilon}(\mathbf{u}^{\text{ex}}) \, d\Omega} \right)^{1/2} \quad (72)$$

is plotted in Figure 19. For the topological enrichment only the nodes whose support is touching the crack tip are enriched. In the case of the geometrical enrichment, nodes within a distance of  $r_e = 0.05$  from the crack tip are enriched.

It can be observed that the convergence rate is 0.5 when the topological or no enrichment is present. The topological enrichment does however yield a smaller error compared to the classical method. But one also observes a marked difference in the trend of the error with geometrical enrichment, which converges at a rate of 1.0.

In order to analyze these convergence rates, we must recall the convergence rate result of the classical finite element method (see for instance Bathe (1996))

$$\epsilon = O(h^{\min(r-m, p+1-m)}) \quad (73)$$

The regularity of the solution is indicated by  $r$  ( $\mathbf{u}^{\text{ex}} \in H^r(\Omega)$ ) whereas  $p$  is the degree of the finite element interpolation and  $m$  is the error norm used. For the benchmark,  $r = 3/2$ ,  $p = 1$  and  $m = 1$ , so we cannot expect a rate greater than 0.5 for the classical FEM. The topological enrichment yields a lower error than a standard FEM analysis because the X-FEM approximation spans a larger space than the FEM one. However, it does not affect the asymptotic convergence rate since the enrichment area goes to zero as the mesh size goes to zero.

With a geometrical enrichment strategy, the enrichment is able to adequately represent (even as  $h$  to zero) the rough part of the solution. The classical part of the approximation is thus only in charge of the smooth part of the solution, yielding the order 1 convergence rate. This was proved by Laborde et al. (2005). It was also shown in this paper that (for the benchmark problem) if the polynomial approximation is raised, higher (still optimal) convergence rates are obtained. The polynomial degree only needs to be raised in the classical part and Heaviside parts of the approximation (the first and second term terms one the right side of (33)).

### 5.4. Conditioning

When solving a linear system of equation  $Kx = f$ , an important number to take into account is the condition number defined as the ratio between the maximum and minimum eigenvalues of the  $K$  matrix.

$$\kappa = \frac{\lambda_{\max}}{\lambda_{\min}} \quad (74)$$

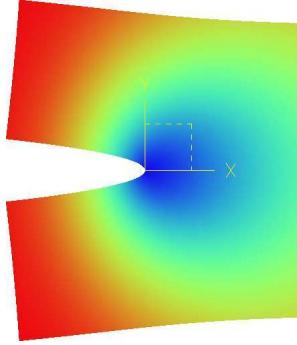


Figure 18: Mode I benchmark problem: deformed shape (with displacements magnified) of a square slab under mode one loading.

This condition number has a direct impact on the convergence rate for an iterative solver and on the propagation of round offs for a direct solver. For instance, for the conjugate gradient iterative solver, the error at iteration  $m$  reads (Saad (2000)):

$$\|x - x_m\|_K \leq 2 \left[ \frac{\sqrt{\kappa} - 1}{\sqrt{\kappa} + 1} \right]^m \|x - x_0\|_K \quad (75)$$

where  $x_0$  is the initial guess,  $x_m$  the iterate  $m$  and

$$\|a\|_K = \sqrt{a^T K a} \quad (76)$$

Thus the higher the condition number, the slower the convergence. To be precise, the bound (34) is in general pessimistic. Indeed, first of all  $\kappa$  can be calculated on the basis of the eigenvalues for which the corresponding eigenvector projected on the right hand side is not zero. Then, the  $\kappa$  can be reajusted progressively with the iterations while being based only on the eigenvectors remaining active through the iterations (for additional details, see Saad (2000)).

The conditioning of the X-FEM was studied in Béchet et al. (2005) and Laborde et al. (2005) for the two types of enrichment strategies: topological and geometrical. The evolution of the condition number according to the size of elements of the grid is given in Figure 20 for the stiffness and mass matrices. They are plotted for the benchmark problem already discussed in section 5.3.

We note that for geometrical enrichment, the condition number grows dramatically with the mesh size. A specific preconditioner was designed in Béchet et al. (2005) to circumvent the increase. The effect of the preconditioner is also given in Figure 20. This preconditioner could be called pre-preconditioner X-FEM preconditioner because it takes care of the specificity of the X-FEM. After its application, a standard FEM preconditioner may be used. The idea behind

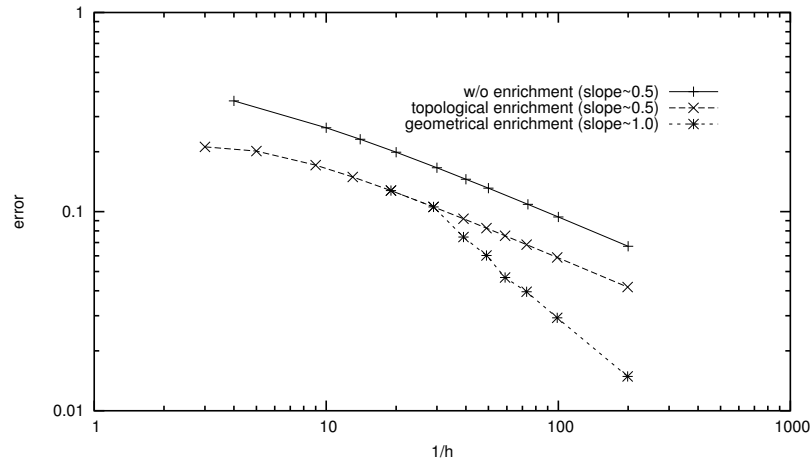


Figure 19: Relative error in the energy norm for the mode I benchmark problem. The top curve corresponds to no enrichment (slope 0.5). The middle curve is the result for topological enrichment, whereas the bottom curve (slope 1) corresponds to the use of geometrical enrichment.

the X-FEM preconditioner is quite simple. On enriched nodes, the enriched shape functions are orthogonalized with respect to the classical shape functions. The matrices related to a given node are thus diagonal.

### 5.5. Stiff interface

At this stage, we did only consider Neumann type boundary conditions on external boundaries of the domain. These type of conditions are easily accounted for in a displacement based variational formulation. The normal stress is simply integrated against the trial displacement. Consider now, a Dirichlet boundary condition imposed on an interface denoted  $\Gamma$ , as in Figure 21. The imposed displacement is assumed to be a zero vector. Two scenarios are depicted whether  $\Gamma$  is meshed or not. In the left case, the number of degrees of freedom is 12 (16 initially minus 6 for the Dirichlet boundary condition). For the right case, a strict enforcement of the Dirichlet requires the displacement to be zero at points A to E. The displacement in the bottom layer of elements thus depend on only two degrees of freedom and the corresponding strain is uniform along  $\Gamma$ . This would be the case even if we considered many more elements. The total number of degrees of freedom for the right case is thus 8 and no longer 12.

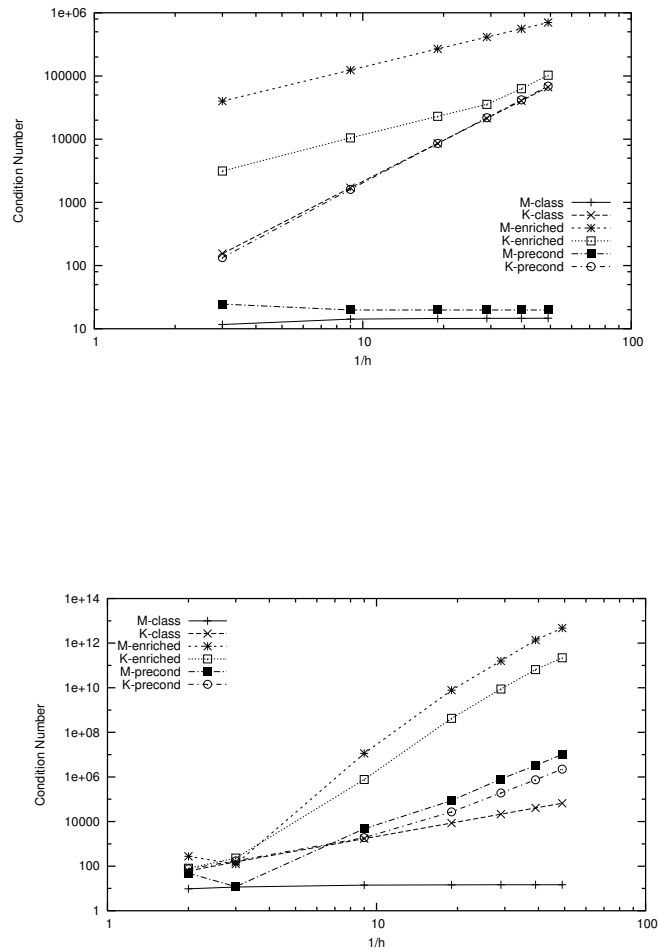


Figure 20: Condition number as a function of the mesh size for the mass and stiffness matrices. Topological (top) and geometrical (bottom) enrichments are considered as well as the influence of the preconditioner.

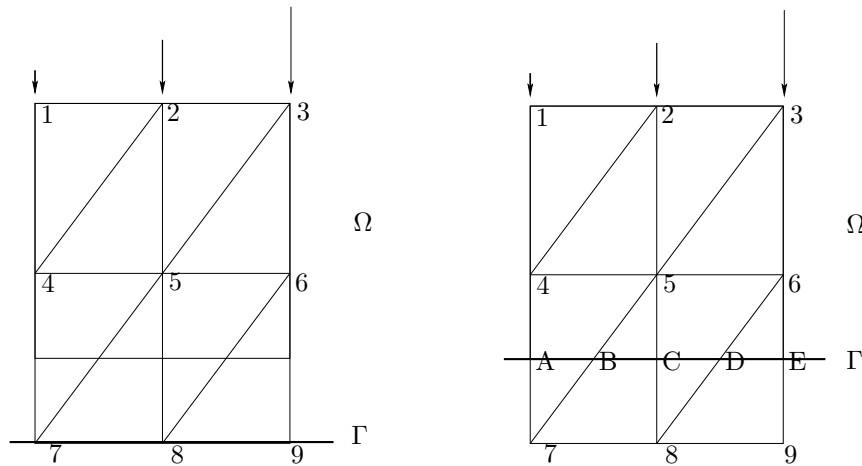


Figure 21: A domain  $\Omega$  with a Dirichlet boundary condition on  $\Gamma$  and Neumann type boundary conditions elsewhere. For the left figure,  $\Gamma$  is fitted with the mesh whereas it is not on the right.

The numerical approximation locks because it can only model a uniform strain and stress along  $\Gamma$ , whereas the solution may be more complex. The left case is able to model varying strain and stress along  $\Gamma$ . This locking phenomena when strongly enforcing Dirichlet boundary conditions within the X-FEM was first noticed by 21. The locking is also clearly exhibited if Lagrange multipliers are used to enforce zero displacements at points A to E. The multipliers suffers from strong oscillations.

Locking is related to stiff interface conditions. It also appears when contact is considered as well as Robin type conditions with a sufficiently large stiffness. A set of papers have been devoted to alleviate this issue, following different strategies:

- following a Nitsche type approach Nitsche (1971); Hansbo and Hansbo (2002b, 2004)
- following a residual-free bubble stabilization approach Mourad et al. (2007); Dolbow and Franca (2008)
- following a Barbosa and Hughes type stabilization of the Lagrange multipliers Haslinger and Renard (2009)
- using a mortar based approach Kim et al. (2007)
- proper choice of the Lagrange multiplier space Moës et al. (2006), Géniaut et al. (2007) and more recently B chet et al. (2009).

The above approaches have in common the fact that they relax the constraint by enforcing it weakly. Obviously the constraint cannot be relaxed too much if optimal rates of convergence are still desired. This trade-off between the rate of convergence and locking is related to the well known LBB or Inf-Sup condition.

We will now detail the later paper B chet et al. (2009) for which the Lagrange multiplier field is discretized using the same nodes as the displacement field.

The nodes of all elements cut by the interface will bear a Lagrange multiplier degree of freedom (these nodes are numbered from 4 to 9 in Figure 21). It was proved in B chet et al.

(2009) that by applying specific ties between the pressure degrees of freedom, the inf-sup condition can be satisfied.

The algorithm to create the ties goes as follows. Let  $E$  be the set of edges cut by the crack. We pick in  $E$  a set of independent edges. Two edges are said to be independent if they do not share a common node. Note that the choice of independent edges is not unique. In Figure 21, the set may be for instance 5-7,6-8 or 4-7,6-8 or even 4-7,5-8,6-9. On the more complex mesh depicted in Figure 22, a possible set of independent edges is indicated by dots (and square at the end nodes).

The Lagrange multiplier degrees of freedom at the end nodes of each independent edge are forced to be equal. This is illustrated by the numbers which are the same in Figure 22 (top), for the end nodes of each independent edge.

Once the independent edges have been selected, some nodes of edges in  $E$  may not have been taken care of. This is the case for the circled nodes in Figure 22 (bottom). The Lagrange multiplier value at these nodes is linked to the value at the squared nodes to which it is connected to through an edge in  $E$  (when the squared are multiple, either one is picked or a linear combination may be built with coefficients forming a partition of unity Béchet et al. (2009)). The algorithm described above may also be applied in 3D. Once the Lagrange multiplier space has been built, it may be used in a classical manner to integrate the bilinear form along the interface.

### 5.6. Nitsche's Method

Nitsche's method is a stabilized method for enforcing constraints on surfaces. Nitsche's method can be viewed as a variationally consistent penalty method, with the advantage that the discrete system of equations are better conditioned provided the method parameters are chosen appropriately. As a result of the pioneering work of Hansbo and Hansbo [?], the method has become popular for a wide class of interface problems. See, for example, the work of Dolbow and Harari [?] in the context of embedded finite element methods, Burman and Hansbo [?] for fictitious domain finite element methods, Becker et al. [?] for incompressible inelasticity, Burman and Fernandez [?], Sanders et al. [?] for fluid-structure interaction, and Zunino et al. [?] for reaction-diffusion equations.

## 6. Further readings

The literature on the X-FEM and GFEM is quite vast and we cannot mention here all interesting papers published.

In terms of fundamental issues, one may cite for instance the issue of incompressibility Dolbow and Devan (2004); Legrain et al. (2008), the issue of friction on crack faces Amdouni et al. (2014), the design of appropriate a posteriori error estimation Strouboulis et al. (2006); Duflo and Bordas (2008); Rodenas et al. (2008) and, finally, the design of well suited enrichment functions Asadpoure and Mohammadi (2007); Chevaugeon et al. (2013). The paper cited above are only examples of references on the topic.

The variety of areas covered by the X-FEM/GFEM is also quite large. We may cite: surgical cuts Vigneron et al. (2004), phase change and solidification Merle and Dolbow (2002); Ji et al. (2002); Chessa et al. (2002), powder compaction Khoei et al. (2006, 2007), geological faults

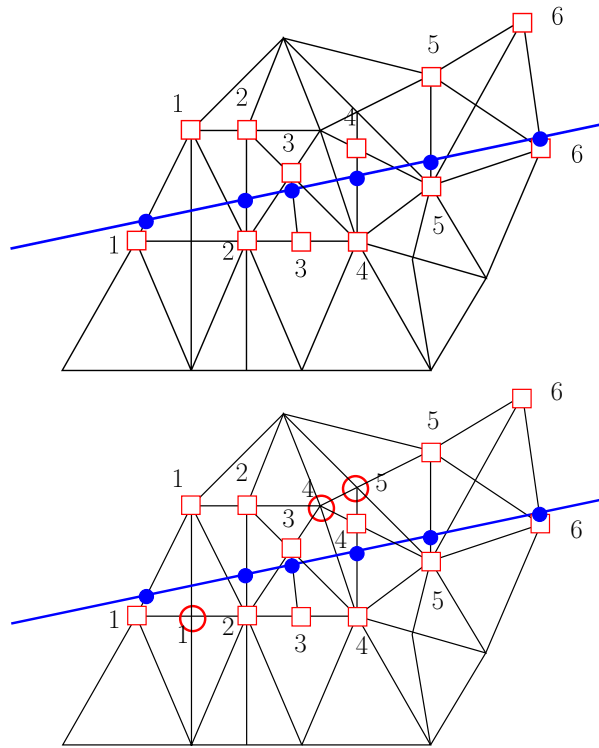


Figure 22: (Top) Selection of the independent edges. These edges are in between square nodes. The connected squared nodes will have the same Lagrange multiplier degrees of freedom. (Bottom) Isolated nodes are located by circle nodes. Their pressure degree of freedom is forced equal to the one of a square they can connect to through a cut edge.

Siavelis et al. (2013), tectonic plate subduction Zlotnik et al. (2007). These are only a fraction of areas covered but they already give an idea of the numerical need in terms of modeling moving interfaces.

#### references

Amdouni, S., Moakher, M., and Renard, Y. (2014). A stabilized Lagrange multiplier method for the enriched finite-element approximation of Tresca contact problems of cracked elastic bodies. *Computer Methods in Applied Mechanics and Engineering*, 270:178–200.

Areias, P. M. A. and Belytschko, T. (2006). Letter to the Editor. *Computer Methods in Applied Mechanics and Engineering*, 195:1275–1276.

Asadpoure, A. and Mohammadi, S. (2007). Developing new enrichment functions for crack

*Encyclopedia of Computational Mechanics*. Edited by Erwin Stein, René de Borst and Thomas J.R. Hughes.

© 2004 John Wiley & Sons, Ltd.

- simulation in orthotropic media by the extended finite element method. *International Journal for Numerical Methods in Engineering*, 69(August 2006):2150–2172.
- Babuška, I. and Melenk, J. M. (1997). The partition of unity method. *International Journal for Numerical Methods in Engineering*, 40:727–758.
- Bathe, K. J. (1996). *Finite element procedures*. Prentice-Hall.
- Béchet, E., Minnebo, H., Moës, N., and Burgardt, B. (2005). Improved implementation and robustness study of the X-FEM for stress analysis around cracks. *International Journal for Numerical Methods in Engineering*, 64(8):1033–1056.
- Béchet, E., Moës, N., and Wohlmuth, B. (2009). A stable Lagrange multiplier space for stiff interface conditions within the extended finite element method. *International Journal for Numerical Methods in Engineering*, 78(8):931–954.
- Belytschko, T., Gracie, R., and Ventura, G. (2009). A review of extended/generalized finite element methods for material modeling. *Modelling and Simulation in Materials Science and Engineering*, 17(4):043001.
- Cano, A. and Moreno, C. (2015). A new method for numerical integration of singular functions on the plane. *Numerical Algorithms*, 68(3):547–568.
- Chessa, J., Smolinski, P., and Belytschko, T. (2002). The extended finite element method (xfem) for solidification problems. *International Journal for Numerical Methods in Engineering*, 53:1959–1977.
- Chevaugéon, N., Moës, N., and Minnebo, H. (2013). Improved crack tip enrichment functions and integration for crack modelling using the eXtended Finite Element Method. *International Journal for Multiscale Computational Engineering*, 11(6):597–631.
- Chopp, D. L. and Sukumar, N. (2003). Fatigue crack propagation of multiple coplanar cracks with the coupled extended finite element/fast marching method. *Int. J. Engineering Science*, 41(8):845–869.
- Colombo, D. and Massin, P. (2010). Fast and robust level set update for 3-D non planar X-FEM crack propagation modelling. *COMPUTER METHODS IN APPLIED MECHANICS AND ENGINEERING*.
- Destuynder, P., M., D., and S., L. (1983). On a numerical method for fracture mechanics. In *Lecture notes in physics*, volume 1121, pages 69–84. Springer.
- Dolbow, J. and Devan, A. (2004). Enrichment of enhanced assumed strain approximations for representing strong discontinuities: addressing volumetric incompressibility and the discontinuous patch test. *International Journal For Numerical Methods in Engineering*, 21(April 2003):1–21.
- Dolbow, J. E. and Franca, L. P. (2008). Residual-free bubbles for embedded Dirichlet problems. *Computer Methods in Applied Mechanics and Engineering*, 197(45-48):3751–3759.

- Duffy, M. G. (1982). Quadrature over a pyramid or cube of integrands with a singularity at a vertex. *SIAM Journal on Numerical Analysis*, 19(6):1260–1262.
- Duflot, M. (2007). A study of the representation of cracks with level sets. *International Journal for Numerical Methods in Engineering*, 70(11):1261 – 1302. Penny-shaped crack; Displacement field; Level set method;
- Duflot, M. and Bordas, S. (2008). A posteriori error estimation for extended finite elements by an extended global recovery. *International Journal for Numerical Methods in Engineering*, 76(8):1123–1138.
- Fries, T. P. and Belytschko, T. (2010). The extended/generalized finite element method: An overview of the method and its applications. *International Journal for Numerical Methods in Engineering*, 84(3):253–304.
- Géniat, S., Massin, P., and Moës, N. (2007). A stable 3D contact formulation for cracks using x-fem. *Revue européenne de mécanique numérique*. To appear.
- Gordeliy, E. and Peirce, A. (2015). Enrichment strategies and convergence properties of the XFEM for hydraulic fracture problems. *Computer Methods in Applied Mechanics and Engineering*, 283:474–502.
- Gravouil, A., Moës, N., and Belytschko, T. (2002). Non-planar 3D crack growth by the extended finite element and level sets? Part II: Level set update. *International Journal for Numerical Methods in Engineering*, 53(11):2569–2586.
- Hansbo, A. and Hansbo, P. (2002a). An unfitted finite element method, based on Nitsche’s method, for elliptic interface problems. *Computer Methods in Applied Mechanics and Engineering*, 191:5537–5552.
- Hansbo, A. and Hansbo, P. (2002b). An unfitted finite element method, based on Nitsche’s method, for elliptic interface problems. *Computer Methods In Appl. Mechanics Engineering*, 191:5537–5552.
- Hansbo, A. and Hansbo, P. (2004). A finite element method for the simulation of strong and weak discontinuities in solid mechanics. *Computer Methods In Applied Mechanics And Engineering*, 193:3523–3540.
- Haslinger, J. and Renard, Y. (2009). A New Fictitious Domain Approach Inspired by the Extended Finite Element Method. *SIAM Journal on Numerical Analysis*, 47(2):1474–1499.
- Holdych, D. J., Noble, D. R., and Secor, R. B. (2008). Quadrature rules for triangular and tetrahedral elements with generalized functions. *International Journal for Numerical Methods in Engineering*, 73(9):1310–1327.
- Huang, R., Prévost, J.-H., Huang, Z. Y., and Suo, Z. (2003). Channel-cracking of thin films with the extended finite element method. *Engineering Fracture Mechanics*, 70(18):2513–2526.
- Hyman, M. A. (1952). Non-iterative numerical solution of boundary-value problems. *Applied Scientific Research, Section B*, 2(1):325–351.

- Ji, H., Chopp, D. L., and Dolbow, J. (2002). A hybrid extended finite element/level set method for modeling phase transformations. *International Journal For Numerical Methods in Engineering*, 54:1209–1233.
- Khoei, A. R. (2015). *Extended Finite Element Method: Theory and Applications*. Wiley Series in Computational Mechanics, New York, N.Y.
- Khoei, A. R., Anahid, M., and Shahim, K. (2007). An extended arbitrary LagrangianEulerian finite element modeling (X-ALEFEM) in powder forming processes. *Journal of Materials Processing Technology*, 188:397–401.
- Khoei, A. R., Shamloo, A., and Azami, A. R. (2006). Extended finite element method in plasticity forming of powder compaction with contact friction. *International Journal of Solids and Structures*, 43:5421–5448.
- Kim, T. Y., Dolbow, J., and Laursen, T. (2007). A mortared finite element method for frictional contact on arbitrary interfaces. *Computational Mechanics*, 39(3):223–235.
- Laborde, P., Pommier, J., and Renard, Y. (2005). High-order extended finite element method for cracked domains. *for Numerical Methods*, pages 1–31.
- Legrain, G., Moes, N., and Huerta, A. (2008). Stability of incompressible formulations enriched with X-FEM. *Computer Methods in Applied Mechanics and Engineering*, 197(21-24):1835–1849.
- Melenk, J. M. and Babuška, I. (1996). The partition of unity finite element method: Basic theory and applications. *Computer Methods in Applied Mechanics and Engineering*, 139:289–314.
- Merle, R. and Dolbow, J. (2002). Solving thermal and phase change problems with the extended finite element method. *Computational mechanics*, pages 1–22.
- Minnebo, H. (2012). Three-dimensional integration strategies of singular functions introduced by the XFEM in the LEFM. *International Journal for Numerical Methods in Engineering*, 92:1117–1138.
- Moës, N., Béchet, E., and Tourbier, M. (2006). Imposing essential boundary conditions in the extended finite element method. *International Journal for Numerical Methods in Engineering*, 67:1641–1669.
- Moës, N. and Belytschko, T. (2002). Extended finite element method for cohesive crack growth. *Engineering Fracture Mechanics*, 69(7):813–833.
- Moës, N., Cloirec, M., Cartraud, P., and Remacle, J.-F. (2003). A computational approach to handle complex microstructure geometries. *Computer Methods in Applied Mechanics and Engineering*, 192(28-30):3163–3177.
- Moës, N., Dolbow, J., and Belytschko, T. (1999). A finite element method for crack growth without remeshing. *International Journal for Numerical Methods in Engineering*, 46(1):131–150.

- Mohammadi, S. (2008). *Extended Finite Element Method for Fracture Analysis of Structures*. Blackwell Publishing, Malden, MA.
- Molino, N., Bao, Z., and Fedkiw, R. (2004). A virtual node algorithm for changing mesh topology during simulation. *ACM Transactions on Graphics (TOG)*, 1(212):385–392.
- Mourad, H. M., Dolbow, J., and Harari, I. (2007). A bubble-stabilized finite element method for Dirichlet constraints on embedded interfaces. *Int. J. For Numerical Methods In Engineering*, 69(4):772–793.
- Mousavi, S. E. and Sukumar, N. (2010a). Generalized Duffy transformation for integrating vertex singularities. *Computational Mechanics*, 45(2–3):127–140.
- Mousavi, S. E. and Sukumar, N. (2010b). Generalized Gaussian quadrature rules for discontinuities and crack singularities in the extended finite element method. *Computer Methods in Applied Mechanics and Engineering*, 199(49–52):3237–3249.
- Nitsche, J. (1971). ber ein variationsprinzip zur lsung von dirichlet-problemen bei verwendung von teilrumen, die keinen randbedingungen unterworfen sind. *Abhandlungen aus dem Mathematischen Seminaren des Universitt Hamburg*, 36:9–15.
- Pommier, S., Gravouil, A., Combescure, A., and Moës, N. (2011). *Extended finite element method for crack propagation*. Wiley.
- Rodenas, J., Gonzalez-estrada, O., Tarancon, J., and Fuenmayor, F. (2008). A recoverytype error estimator for the extended finite element method based on singular+ smooth stress field splitting. *International journal for numerical methods in engineering*, 76(March):545–571.
- Saad, Y. (2000). *Iterative methods for sparse linear systems*. PWS Publishing company, third edition edition.
- Sethian, J. (1999). *Level set methods and fast marching methods: Evolving interfaces in computational geometry, fluid mechanics, computer vision and material science*. Cambridge University Press.
- Shi, J., Chopp, D., Lua, J., Sukumar, N., and Belytschko, T. (2010). Abaqus implementation of extended finite element method using a level set representation for three-dimensional fatigue crack growth and life predictions. *Engineering Fracture Mechanics*, 77(14):2840–2863.
- Siavelis, M., Guiton, M., Massin, P., and Moës, N. (2013). Large sliding contact along branched discontinuities with X-FEM. *Computational Mechanics*, 52:201–219.
- Simo, J. C., Oliver, J., and Armero, F. (1993). An analysis of strong discontinuities induced by strain-softening in rate-independent inelastic solids. *Computational Mechanics*, 12:277–296.
- Song, J., Areias, P. M. A., and Belytschko, T. (2006). A method for dynamic crack and shear band propagation with phantom nodes. *International Journal For Numerical Methods in Engineering*, 67(December).

- Stolarska, M., Chopp, D. L., Moës, N., and Belytschko, T. (2001). Modelling crack growth by level sets in the extended finite element method. *International Journal for Numerical Methods in Engineering*, 51(8):943–960.
- Strouboulis, T., Copps, K., and Babuška, I. (2001). The generalized finite element method. *Computer Methods in Applied Mechanics and Engineering*, 190(32–33):4081–4193.
- Strouboulis, T., Zhang, L., Wang, D., and Babuška, I. (2006). A posteriori error estimation for generalized finite element methods. *Computer Methods in Applied Mechanics and Engineering*, 195(9–12):852–879.
- Sukumar, N., Chopp, D. L., Béchet, E., and Moës, N. (2008). Three-dimensional non-planar crack growth by a coupled extended finite element and fast marching method. *International Journal for Numerical Methods in Engineering*, 76(5):727–748.
- Sukumar, N., Chopp, D. L., and Moran, B. (2003). Extended finite element method and fast marching method for three-dimensional fatigue crack propagation. *Engineering Fracture Mechanics*, 70:29–48.
- Sukumar, N., Dolbow, J. E., and Moës, N. (2015). Extended finite element method in computational fracture mechanics: A retrospective examination. *International Journal of Fracture*, 196(1–2):189–206.
- Sukumar, N., Moës, N., Moran, B., and Belytschko, T. (2000). Extended finite element method for three-dimensional crack modelling. *International Journal for Numerical Methods in Engineering*, 48(11):1549–1570.
- Ventura, G. and Benvenuti, E. (2015). Equivalent polynomials for quadrature in Heaviside function enriched elements. *International Journal for Numerical Methods in Engineering*, 102(3–4):688–710.
- Ventura, G., Budyn, E., and Belytschko, T. (2003). Vector level sets for description of propagating cracks in finite elements. *International Journal for Numerical Methods in Engineering*, 58:1571–1592.
- Vigneron, L. M., Verly, J. G., and Warfield, S. K. (2004). On {Extended} {Finite} {Element} {Method} {(XFEM)} for modelling of organ deformations associated with surgical cuts. *Medical Simulation, Proc.*, 3078:134–143.
- Zhuang, Z., Liu, Z., Cheng, B., and Liao, J. (2014). *Extended Finite Element Method*. Tsinghua University Press Computational Mechanics Series, Beijing, China.
- Zi, G. and Belytschko, T. (2003). New crack-tip elements for XFEM and applications to cohesive cracks. *International Journal For Numerical Methods in Engineering*, 57(January):2221–2240.
- Zlotnik, S., Diez, P., Fernández, M., and Vergés, J. (2007). Numerical modelling of tectonic plates subduction using X-FEM. *Computer Methods in Applied Mechanics and Engineering*, 196:4283–4293.